THROAT STABILITY-BYPASS SYSTEMS TO INCREASE THE STABLE AIRFLOW RANGE OF A MACH 2.5 INLET WITH 60-PERCENT INTERNAL CONTRACTION

by Glenn A. Mitchell, Bobby W. Sanders, and Robert J. Shaw

Lewis Research Center
Cleveland, Ohio 44135

NATIONAL AERONAUTICS AND SPACE ADMINISTRATION • WASHINGTON, D. C. • JULY 1974

1. Report No. NASA TM X-2976	2. Government Accession No.	3. Recipient's Catalog No.
4. Title and Subtitle THROAT STABILITY-BYPASS SYSTEMS TO INCREASE THE STABLE AIRFLOW RANGE OF A MACH 2.5 INLET WITH 60-PERCENT INTERNAL CONTRACTION		5. Report Date JULY 1974
		6. Performing Organization Code
7. Author(s) Glenn A. Mitchell, Bobby W. Sanders, and Robert J. Shaw		8. Performing Organization Report No. E-7738
9. Performing Organization Name and Address Lewis Research Center National Aeronautics and Space Administration Cleveland, Ohio 44135		10. Work Unit No. 501-24
		11. Contract or Grant No.
		13. Type of Report and Period Covered Technical Memorandum
12. Sponsoring Agency Name and Address National Aeronautics and Space Administration Washington, D.C. 20546		
		14. Sponsoring Agency Code

15. Supplementary Notes

16. Abstract

The results of an experimental investigation to increase the stable airflow range (without unstart) of a supersonic mixed-compression inlet are presented. Various stability bypass entrances were located on the cowl side of the inlet throat. The types of entrance were distributed porous (normal holes), forward-slanted slot, and distributed educated slots. A large stable airflow range was obtained for each entrance type if a constant pressure was maintained in the stability bypass plenum. The distributed porous entrance provided the largest stable airflow range. Inlet unstart angle of attack was unaffected by the entrances.

17. Key Words (Suggested by Author(s)) Air intake; Supersonic cruise inlets; Shock stability; Inlet bleed; Throat-bypass bleed; Throat stability bypass	18. Distribution Statement Unclassified - unlimited Category 01		
19. Security Classif. (of this report) Unclassified	20. Security Classif. (of this page) Unclassified	21. No. of Pages 42	22. Price* $3.25

THROAT STABILITY-BYPASS SYSTEMS TO INCREASE THE STABLE

AIRFLOW RANGE OF A MACH 2.5 INLET WITH

60-PERCENT INTERNAL CONTRACTION

by Glenn A. Mitchell, Bobby W. Sanders, and Robert J. Shaw

Lewis Research Center

SUMMARY

An experimental investigation was conducted to evaluate the effectiveness of various types of stability bypass entrances, located in the inlet throat, to provide an increased inlet stable airflow range. The inlet used for this study was an axisymmetric mixed-compression type with 60 percent of the supersonic area contraction occurring internally at the design Mach number of 2.5. Data were obtained at this design Mach number for three stability bypass entrance types: distributed porous, forward-slanted slot, and distributed educated slots

With the inlet operating at a high-performance condition, each of the stability-bypass entrance types provided a large stable airflow range before inlet unstart. In terms of diffuser-exit corrected airflow, each type of entrance provided a reduction, before unstart, of 15 percent or greater if a constant pressure was maintained in the stability-bypass plenum. The distributed porous entrance provided the largest stable airflow range of 25.5 percent and controlled the cowl-side boundary layer better than other entrance types. Inlet unstart angle-of-attack tolerance was unaffected by the presence of the bypass entrances.

INTRODUCTION

At flight speeds above Mach 2.0 an inlet having a mixture of internal and external compression offers high performance by supplying the engine with airflow at a high pressure level while maintaining low drag. To provide optimum internal performance for this type of inlet, the terminal shock must be kept at the inlet throat. However, mixed-compression inlets suffer from an undesirable airflow characteristic known as unstart.

The closer the terminal shock to the throat, the smaller the disturbance that will cause an unstart to occur. This airflow disturbance causes the terminal shock to move forward of the throat where it is unstable and is violently expelled ahead of the inlet cowling. This shock expulsion or unstart causes a large rapid reduction in both mass flow and pressure recovery, and thus a large thrust loss and drag increase. Inlet buzz, compressor stall, and/or combustor blowout may also occur. Obviously, an inlet unstart is extremely undesirable, not only because of the effects on the propulsion system itself, but also on the aerodynamic qualities of the aircraft. If an inlet unstart does occur, large variations of the inlet geometry are required to re-establish initial design operating conditions.

Both external airflow transients such as atmospheric turbulence and internal airflow changes such as a reduction in engine airflow demand can cause the inlet to unstart. It is desirable for the inlet to have a sufficiently large stable margin to absorb such transients without unstarting. For an internal airflow change the inlet should provide a margin in corrected airflow below the value for optimum performance without incurring unstart. This margin is defined as the stable airflow operating range. Conventional mixed-compression inlets can be designed to have some stable range that is provided by the capacity of the performance bleed systems. Since performance bleed exit areas are generally fixed, this stable range may not be adequate to absorb many of the airflow transients that are encountered by a typical supersonic propulsion system. An increased stable airflow range may be provided by operating supercritically with a resultant loss in performance. Since any loss in performance is reflected directly as a loss in thrust, supercritical operation should be avoided.

To provide the necessary stable airflow range without compromising steady-state performance, the inlet can be designed to replace the throat bleed with a stability-bypass system capable of removing large amounts of airflow when needed. This system prevents unstarts by increasing bypass airflow to compensate for reductions in the diffuser exit airflow demand. References 1 and 2 indicate that large increases in this bypass airflow may be provided without prohibitive amounts of airflow removal during normal operation. These increases in bypass airflow occur when the exit area is controlled to maintain a relatively constant pressure in the bypass plenum. This bypass exit area variation might either be provided by an active control using shock positions sensors, or by a passive control such as pressure-activated valves. These valves would open in response to the pressure rise in the bypass plenum caused by the forward moving terminal shock. To be the most effective, the valves should be designed to maintain a nearly constant stability-bypass plenum pressure. Using a Mach 2.5 mixed-compression inlet with 40-percent internal contraction, reference 2 reported that several types of stability-bypass entrance configurations were capable of providing a large stable airflow range if a constant-pressure bypass exit control could be used. When these stability-bypass

2

entrance configurations were used with pressure-activated valves (refs. 3 and 4), the diffuser-exit airflow could be reduced as much as 28 percent from the optimum performance point without causing inlet unstart.

Experimental tests were conducted in the Lewis 10- by 10-Foot Supersonic Wind Tunnel to continue the evaluation of stability-bypass systems. The same types of stability-bypass systems as used in references 3 and 4 were investigated using an axisymmetric, Mach 2.5, mixed-compression inlet having 60 percent of the design supersonic area contraction occurring internally. Stability-bypass airflow was removed from the cowl surface of the inlet throat region through several alternate stability-bypass entrance configurations. These configurations used either a distributed porous surface, distributed educated slots, or a forward-slanted slot. The detailed performances of the various stability-bypass configurations of each type of entrance are reported in references 5 to 7. The steady-state inlet stability limits that were obtained for the best configuration of each bypass entrance type are compared herein to determine their suitability for use with pressure-activated valves in controlling a downstream disturbance. Data were obtained at a free-stream Mach number of 2.5 and a Reynolds number, based on inlet cowl lip diameter, of 3.88×10^6.

U.S. Customary Units were used in the design of the test model and for the recording and computing of experimental data. These units were converted to the International System of Units for presentation in this report.

APPARATUS AND PROCEDURE

Inlet Model

The inlet used in this investigation was a Mach 2.5, axisymmetric, mixed-compression type with 60 percent of the design supersonic area contraction occurring internally. The inlet capture area of 0.1758 square meter sized the inlet to match the airflow requirements of the J85-GE-13 engine at Mach 2.5 and at a free-stream temperature of 390 K. The inlet was attached to a 0.635-meter-diameter cylindrical nacelle in which the J85-GE-13 engine or a coldpipe choked-exit plug assembly could be installed. For this study only the coldpipe was used. Figure 1 shows the test model installed in the wind tunnel test section.

Some of the basic inlet design details are presented in figure 2. Cowl and center-body static-pressure distributions, inlet contours, and diffuser area variations are shown for the inlet design Mach number and spike position. External compression was accomplished with a 12.5° half-angle cone (fig. 3). Translation of this conical center-body provided a varying contraction ratio for off-design operation and inlet restart. At

design conditions the cone tip oblique shock passed just ahead of the cowl lip so that approximately 0.25 percent of the capture airflow was spilled over the lip. Internal compression was accomplished with the oblique shock generated by the 0° cowl lip and the two reflected oblique shocks plus isentropic compression between these reflected shocks. As was pointed out in reference 8, the actual oblique shock reflection points were forward of the theoretically predicted points. The geometric throat of the inlet was located at x/R_c = 3.475 inlet radii (centerbody surface) where the theoretical average supersonic Mach number was 1.239 with a total-pressure recovery of 0.988. Behind the terminal shock the theoretical recovery was 0.975 at a Mach number of 0.8125.

The subsonic diffuser consisted of an initial throat region 4 hydraulic radii long with a 1^O equivalent conical expansion followed by the main diffuser having an equivalent conical expansion of 8°. The aft portion of the diffuser incorporated two remotely controlled bypass systems: a high-response overboard system for shock position control and a low-speed ejector bypass for engine and nozzle cooling airflow (fig. 3). For the data reported herein both of these bypass systems were closed. The overboard bypass system leaked about 1 percent of the capture mass flow when nominally closed. The cascades placed at the entrance of the overboard bypass cavity (fig. 3) were found in reference 9 to minimize a resonance condition in the cavity. Vortex generators were installed on the centerbody at inlet station 98.07 (fig. 3). Details of the vortex generator design are shown in figure 4.

The overall diffuser length, cone tip to compressor face, was 7.72 cowl lip radii. Internal surface coordinates of the inlet in terms of the cowl lip radius are presented in table I. A more complete discussion of the inlet design characteristics is presented in reference 8.

Bleed regions were located in the throat region of the inlet on the cowl and centerbody surfaces. As shown in figure 5 the bleed at the forward cowl location was dumped directly overboard. Stability-bypass airflow (used to give the inlet a large stable airflow range) was removed through the stability-bypass entrance located on the cowl side of the throat region. Figures 3 and 5 illustrate the ducting of the stability-bypass flow through the cowling to the bypass pipes (fig. 3). Both the cowl stability-bypass flow and the centerbody bleed used two coldpipe choked-plug assemblies each. The remotely actuated plug assemblies that were used to vary these bleed and bypass flows as well as the main duct flow are shown in figure 1(b).

The photographs and sketches of the test model show a bulky external profile, which was necessary to facilitate the major changes made to the stability bypass and associated ducting to vary the entrance configurations. Hence, this configuration is not representative of flight-type hardware.

4

Stability Bypass Entrance and Bleed Region Configurations

The three types of stability bypass entrances that were investigated are shown in figure 6: the distributed porous entrance (fig. 6(a)), the forward-slanted slot entrance (fig. 6(b)), and the distributed educated entrance (fig. 6(c)). The forward cowl bleed was used for a performance bleed and was located forward of each stability-bypass entrance type. As figure 6 shows, the forward cowl bleed was composed of normal holes except when used with the educated configuration and educated slots were used. The design of these basic stability-bypass entrances was, for the most part, based on the bleed characteristic information contained in references 10 to 12. These bleed characteristics and the test data (refs. 1 and 8) were used to determine the location and amount of open bypass entrance area for each of the different entrance types.

The distributed porous entrance was extended across the inlet throat region as shown in figure 6(a), beginning at $x/R_c = 3.282$ inlet radii (just aft of the oblique shock) and ending aft of the throat at $x/R_c = 3.579$ inlet radii. The distributed porous entrance (and the forward cowl bleed region as well) was composed of rows of normal holes as is shown in figure 6(a). The holes were arranged in a concentrated, staggered pattern, which was intended to prevent flow induced circumferential variations in the boundary layer. Holes were 0.3175 centimeter in diameter and were drilled normal to the local inlet surface. A nominal porosity of 40 percent was achieved by locating the holes on 0.4763-centimeter centers. Nominal thickness of the metal surfaces in the bleed region or bypass entrance was equal to the hole diameter. The design provided the bypass entrance with the capability of bleeding 27 percent of the inlet capture mass flow.

The same porous design was also incorporated in the forward cowl bleed that was used with the forward-slanted slot stability-bypass entrance (fig. 6(b)). In concept, a slanted slot entrance is superior to a porous surface entrance in providing a higher pressure recovery. Two slot sizes were designed using the slanted slot concept. The larger one was designed to pass 23 percent of the inlet capture airflow and had a slot height of 1.452 centimeter. The performance of the larger slot is reported in reference 7 where it is compared with smaller slot data. The smaller slot, again reported herein, provided about one half of the bypass entrance area of the larger slot. It was created by adding an insert to the larger slot (as shown in fig. 6(b)). The slot was flush with the local surface and was slanted away from the surface at a 20° angle. The upstream corner of the slot was sharp, and the downstream lip, before rounding, was located at the inlet geometric throat. A round lip was selected for testing on the basis of the effects of lip shape reported in reference 2.

The distributed educated bypass entrance (fig. 6(c)) covered about the same region of the inlet throat as did the distributed porous entrance. With the distributed educated entrance, the forward cowl bleed was composed of educated slots rather than normal

holes. The "educating" technique used herein was an approximation of the ideal rear-ward slanted hole concept. The rear slant or "education" theoretically limits the amount of airflow through the holes when the flow over the perforated area is supersonic. With subsonic flow over the perforated area, the airflow through the holes is relatively unaffected by the slant, and a flow coefficient nearly that of a normal hole is predicted. Because of the difficulty of drilling slanted holes in the cowl surface, a number of circumferential slots were used rather than many holes. To educate these slots, the downstream edge was relieved to obtain a 10° angle with the local surface. The slot width was 0.318 centimeter with 1.27 centimeter between adjacent slots. Local porosity resulting from this arrangement was 25 percent and resulted in a stability-bypass entrance capable of theoretically removing 17 percent of the inlet capture mass flow.

The forward centerbody bleed region is shown in figure 7 and was composed of the same concentrated hole pattern that was used for the distributed porous bypass entrance. There were also five rows of holes aft of the inlet throat. Variations from the basic centerbody bleed pattern shown in figure 7 were accomplished by closing selected rows of holes to create a centerbody bleed arrangement that was compatible with the cowl-side stability-bypass entrance. The development of a compatible centerbody bleed arrangement is reported in reference 5. The final arrangement is shown in figure 8; it consisted of three hole rows upstream and three hole rows downstream of the experimental shock impingement point.

The three basic stability-bypass entrance types were used to create the six bypass configurations that were tested during the investigation. Performances of like types of these configurations are reported in references 5 to 7. The best performing configuration of each bypass entrance type is reported herein and is shown in figure 8. Except for the forward-slanted slot, modification of the basic bypass and bleed arrangements shown in figure 6 was accomplished by changing the open areas by filling selected holes and/or slots. Because of these area modifications, the expected mass flow removal capability of the resulting configurations was reduced from that of the completely open area. The distributed porous configuration reported herein could then theoretically remove 18 percent of the inlet capture mass flow. The educated slot configuration could remove 14 percent and the slot about 11 percent of inlet capture mass flow. The distributed porous configuration reported herein is configuration NH-3 of reference 5. The educated configuration is the same educated configuration reported in reference 6.

Instrumentation

Static-pressure distributions along the top centerline of the inlet cowl and centerbody were measured by the axially located static-pressure instrumentation presented in tables II and III. The main-duct total-pressure instrumentation (fig. 9) was used to

determine the local flow profiles through the inlet and subsonic diffuser. The axial location of these total-pressure rakes is shown in figure 3. Overall inlet total-pressure recovery and distortion were determined from the six 10-tube total-pressure rakes that were located at the diffuser exit (fig. 9(b)). Each rake consisted of six equal-area-weighted tubes with additional tubes added at each side of the extreme tubes in positions corresponding to an 18-tube area-weighted rake. The main duct airflow, the stability-bypass airflow and the centerbody bleed airflow were determined by measurements from the coldpipe choked-exit plug assemblies shown in figure 1(b).

Bleed flow through the forward cowl bleed region was determined from the measured total and static pressures (fig. 9(c)) and the bleed exit area. Stability-bypass total pressure was obtained from two total-pressure rakes that were located in the bypass plenum at an x/R_c of 4.086 inlet radii. Pressures from these rakes were averaged and divided by the free-stream total pressure to obtain the stability-bypass recovery. Centerbody bleed and overboard-bypass total pressures were each measured by a single probe as indicated in figure 9(c).

Forward-slanted slot pressure instrumentation is presented in figure 10. Rake labeling is identical to that of reference 7. Total-pressure rakes were located forward and aft of the upstream corner of the slot and in the slot passage. They were circumferentially indexed to avoid flow interference. Static pressures were also measured axially along the slot and are shown in figure 10.

PERFORMANCE ANALYSIS TECHNIQUE

This section of the report introduces stylized plots (fig. 11) that are typical of actual inlet stability data to be presented later. These plots are used to explain the data presentation and to show the method used to construct a final performance plot. Various performance conditions have been labeled in figure 11 to aid in the discussion.

The stability-bypass performance is shown in figure 11(a) where the total-pressure recovery is presented as a function of the mass-flow ratio of the stability bypass. The series of straight solid lines (A'A B, C'C D etc.) represent the bypass performance obtainable with several different bypass fixed-exit areas. Corresponding inlet performance is presented in figure 11(b) by a series of standard diffuser-exit total-pressure recovery against mass-flow ratio curves. The diffuser-exit mass-flow ratio, of course, reflects changes in bypass mass-flow ratio and also changes in forward cowl and centerbody bleed mass-flow ratio. Each solid-line curve represents the performance obtainable with a fixed bypass exit area and corresponds to the solid straight line of identical labeling in figure 11(a). Each of these curves is generated by reducing the inlet diffuser-exit corrected airflow from a supercritical value and causing the inlet terminal shock to move upstream until unstart occurs. By this mode of operation, loci (dashed curves) of super-

critical stability-bypass airflow (A'A C'C E'E G'G) and minimum stable bypass airflow (BDFH) are obtainable. For a given bypass exit area all the supercritical inlet operating points have approximately the same bypass mass-flow and pressure recovery values. Only when the terminal shock is in the vicinity of the stability-bypass entrance region will shock pressurization occur causing increases in the bypass mass flow and pressure recovery toward their respective minimum stable limit values. Thus, for example, all the inlet operating points between A' and A of figure 11(b) will have the same stability-bypass performance point which is labeled as A'A in figure 11(a).

To assess inlet stability, it is necessary to look at the change in the diffuser-exit corrected airflow, which is a function of both diffuser-exit mass-flow ratio and total-pressure recovery. Figure 11(c) presents inlet stability, expressed as an airflow index, for the same conditions of figures 11(a) and (b). Values of airflow index (AI) represent the percentage change in corrected airflow between any inlet operating condition and the minimum recorded corrected airflow at point H. Figure 11(c) thus illustrates the amount of stable margin available if the stability-bypass exit area can be varied to guide the inlet operation from any operating condition to an unstart at point H. If a fixed exit area was used to obtain the large stability-bypass airflow available at point H (fig. 11(a)), a prohibitively large amount of bypass airflow would be incurred at supercritical conditions (point G). If the fixed-exit area is reduced to obtain an acceptably low level of supercritical bypass airflow (point C), the amount of bypass airflow and consequently the stable margin at the minimum stable condition (point D) is also reduced. Similar bypass characteristics are reported in references 1 to 4.

Data such as presented in figures 11(a) to (c) show the characteristic performance of an inlet with a stability bypass entrance. Since a performance assessment from these plots is difficult, a single operating line was chosen to represent the configuration performance. One end of the line represents a selected inlet match point (point A, e.g.). The match point is chosen to have a high recovery and a small amount of cowl side airflow removal for boundary layer control. The other end of the operating line (the minimum stable point) was chosen by the selection of an ideal variable exit area, one that would provide a constant pressure in the bypass plenum as the inlet operated from match to minimum stable conditions. This variable exit area provides the maximum attainable stability (points A to M in fig. 11(a)). Reference 4 reports a pressure-activated valve that varied stability-bypass exit area to maintain an almost constant bypass plenum pressure. Thus the selection of a constant pressure characteristic for a stability-bypass exit control is a valid technique to assess stability performance.

The inlet stability margin that is produced by a constant-pressure bypass exit control is expressed as a stability index SI_{cp}. Figure 11(d) presents the constant pressure stability index for all of the operating points of figures 11(a) to (c). Note that the selected match point stability (A to M on figs. 11(a) to (c)) is now represented by a single

8

point A. The values of stability index at any operating point represent the percent change in corrected airflow between that point and a minimum stable point that is reached only along a line of constant stability-bypass pressure (A to M in fig. 11). When the inlet operating point has a stability-bypass recovery lower than that of the absolute minimum stable point (H in fig. 11(c)), the absolute minimum stable point is used to compute stability index. Therefore, the stability index for the lower bypass recovery conditions in figure 11(d) becomes identical to the airflow index in figure 11(c). Although the stability index is defined in terms of corrected airflow (see SYMBOLS section), it was simpler in practice to determine values of stability index directly from curves of airflow index by means of the derived equation

$$SI_{cp} = 100 \left(\frac{AI_{op} - AI_{min\ s,\ cp}}{100 - AI_{min\ s,\ cp}} \right)$$

where AI_{op} is the airflow index at any inlet operating condition and $AI_{min\ s,\ cp}$ is the airflow index in figure 11(c) and where a constant bypass pressure line from the operating point intersects the minimum stable curve BDFH. (All symbols are defined in the appendix.)

Constant-pressure stability index may be converted into a typical inlet performance plot like figure 11(g) by means of figures 11(e) and (f). Figure 11(e) presents the constant pressure stability index that was computed for each inlet operating condition as a function of the inlet total-pressure recovery. A selected inlet total-pressure recovery may be represented on figure 11(e) as a dashed vertical line (IJKL). (In these examples, point A is no longer the selected match point.) The intersection of this line with the lines of constant bypass exit area describe the constant-pressure stability indices available at the selected inlet recovery for the various bypass exit areas. A replot of these data in figure 11(f) shows the amount of stability margin that is available when operating the inlet at the selected match recovery as a function of the various amounts of initial total cowl bleed and bypass airflow. Any of the data points in figure 11(f) may be converted into a typical inlet performance plot. Point J, for example, is shown in figure 11(g) and is determined by the previously selected inlet recovery and the initial total cowl and centerbody bleed and the bypass mass-flow ratios. If point J represents critical inlet performance, then supercritical performance is represented by a vertical line extended below point J. The constant-pressure stability index for point J is represented by the airflow difference between two corrected airflow lines; one through the selected match point $(W_{corr})_{op}$, and the other, $(W_{corr})_{min\ s,\ cp}$, intersecting the locus of minimum stable conditions on the inlet performance map. This intersection point is represented in figure 11(b) by the left most extent of the inlet performance curve. Inlet performance

between the match point and the minimum stable point is represented by a straight line. Intermediate points could be determined by using figures 11(a) and (d).

RESULTS AND DISCUSSION

The basic data plots as illustrated by figure 11 are presented in figures 12 to 14 for the distributed porous, the forward-slanted slot, and the distributed educated stability-bypass-entrance configurations. These figures also contain, in addition to the basic plots, the variation of inlet recovery with stability-bypass mass flow, centerbody and forward cowl bleed performance, and compressor face distortion. The variation of inlet recovery with bypass airflow (parts (g) of figs. 12 to 14) is included as an aid to relate the stability-bypass performance (parts (a) of each figure) to the inlet performance (parts (b)). The centerbody and forward cowl bleed mass flow (parts (h)) is necessary to determine the diffuser-exit mass-flow ratios presented in a later summary figure. The distortion (parts (i)) is included to complete the performance presentation of each configuration.

Among the bypass entrance configurations, the best stability bypass performance was provided by the distributed porous configuration. The performance map of this configuration (fig. 12(a)) shows a large available region of operation when compared with the bypass performance map of either the forward-slanted slot configuration (fig. 13(a)) or the distributed educated configuration (fig. 14(a)). The maximum amount of mass flow bypassed by the porous configuration was 0.21 of the capture mass-flow ratio. It was provided at a bypass total-pressure recovery of 0.33. The maximum bypass recovery of this configuration was 0.64.

The bypass performance of the forward-slanted slot configuration, by comparison (fig. 13(a)) provided a maximum mass-flow ratio of 0.11, but at a higher recovery of 0.47. The maximum bypass recovery for the slot configuration was 0.72; the highest of any configuration. Thus the conceptual advantage of a high recovery from the forward-slanted slot was realized. The slot is then an attractive configuration in that drag losses from the bypassed airflow would be lessened compared with the porous configuration, and more flow could be bypassed through a smaller valve.

The bypass performance of the distributed educated bypass entrance configuration was also less than that provided by the porous configuration. The maximum mass-flow ratio achieved was 0.12. But the corresponding total-pressure recovery was a low 0.19 (fig. 14(a)). An examination of figure 14(a) shows that some of the characteristics of "education" were realized by this configuration; that is, the supercritical curve of figure 14(a) was quite low when compared with that of the porous configuration. However, the benefits of this lowered curve were not realized because the bypass performance

10

curve at minimum stable conditions was also much lower. These results were similar to those of an educated configuration reported in reference 2. Thus a very large expected pressure differential (and, therefore, airflow differential) between supercritical and minimum stable operation was not obtained.

A direct comparison of the performance of the bypass entrance configurations can be made by assuming the use of a constant pressure device at the bypass exit and a specific inlet total-pressure recovery. The resulting comparison is presented in figure 15 for a total-pressure recovery of 89 percent. The constant pressure stability index is plotted as a function of the forward cowl bleed plus bypass mass-flow ratio. The data shown are replots of parts (f) of figures 12 to 14. Because of its larger design bypass mass-flow ratio, the porous configuration provided a stability index larger than those of the other configurations.

A more specific comparison of the performance of the bypass configurations can be made from figure 15 by selecting an inlet match condition having a specific forward cowl bleed plus bypass mass-flow ratio. Previous studies have shown that cowl side flow removal of about 2 percent of the inlet capture mass-flow ratio provides good inlet performance (ref. 8). Therefore, this amount was chosen, along with the 89 percent diffuser-exit pressure recovery, as the inlet match condition. This match condition was not intended to be a point of optimum performance for the configurations reported herein; only a reasonable one for comparative purposes. The symbol ● in figure 15 mark the match condition. By using this condition and working backward by linear interpolation through parts (d) and (e) of figures 12 to 14, the bypass performance can be generated. The resulting performance is shown in parts (a) of figures 12 to 14 by the ● and the arrow. With the porous bypass entrance installed and with the inlet operating from the match condition, the bypass airflow could be increased by a mass-flow ratio of 0.18 at a constant bypass recovery of 0.43. Use of the forward-slanted slot bypass entrance provided a bypass mass-flow ratio increase of only 0.10, at a constant recovery of 0.49. The distributed educated entrance provided a bypass mass-flow ratio increase of about 0.08 at a low recovery of 0.36.

The inlet performance provided by the three bypass entrance configurations, with the inlet operating from the selected match condition and with an assumed constant pressure control at the bypass exit, are presented in figure 16. These performance curves were constructed from the data of figures 12 to 15. (Each curve of fig. 16 corresponds to the curve illustrated in fig. 11(g).) The mass-flow ratio for the supercritical portion of the inlet performance curve up to the 89-percent recovery match condition is determined by the initial selected conditions. With these conditions, a constant-pressure stability index was obtained for each configuration from the plots of figure 15. For reference these constant-pressure stability indices are listed in the legend of figure 16. The superiority of the porous bypass configuration in providing a large stable range is

apparent. From the selected match condition, the porous configuration obtained a stability index of 25.5 percent; whereas the slot configuration obtained a smaller index of 18.5 percent and the educated configuration yielded the smallest index of 15.5 percent.

Most of the stability achieved with each configuration resulted from the action of the bypass in removing airflow from the inlet. A minor contribution to the stability came from the increase (from supercritical to minimum stable) in the centerbody bleed flow. In addition to the mass flow removal, an important contribution to the stability came from the increase in inlet total-pressure recovery as the inlet operated from the match condition to minimum stable. As illustrated by parts (b) of figures 12 to 14, the peak inlet total-pressure recovery was 0.95. The use of a constant bypass recovery from the match condition (fig. 16) increased the recovery from 89-percent to nearly the peak value: 94-percent for the porous configuration and 94.4-percent for the other two configurations. These recovery increases provided 16 percent of the stability range achieved with the porous configuration, 27 percent of the range of the slot configuration, and 33 percent of the range of the educated configuration.

In addition to providing the best stability performance, the distributed porous entrance configuration was also superior to the other entrance configurations in minimizing the throat boundary-layer thickness. As illustrated in figure 17 at minimum stable conditions, the forward-slanted slot and distributed educated configurations produced slightly thicker cowl side boundary layers than did the porous configuration. At supercritical conditions (fig. 18) the porous configuration produced a relatively thin, well behaved, boundary layer. The slot and educated configurations on the other hand produced much thicker boundary layers, indicating that the flow was considerably degraded in passing over these entrances.

In assessing the stability performance of the bypass entrance types presented herein, it is well to recall that the porous configuration, in achieving a maximum bypass mass-flow ratio of 0.21, was designed for a mass-flow ratio of 0.18. The slot configuration, which produced a bypass mass-flow ratio of 0.11, was designed for 0.11 mass-flow ratio; the educated configuration, with a maximum mass-flow ratio of 0.12, was designed for a mass-flow ratio of 0.14. Thus all designs obtained close to their design mass flows.

One method of increasing the stability potential of the inferior configurations would be to provide a larger bypass entrance. In the case of the educated configuration a substantial area increase is not possible because the current design uses most of the available throat area. Even if an area increase were possible, the current educated design may not be effective because the benefits of education were not realized in this design. Other designs using the education concept might benefit from a larger entrance. A larger forward-slanted slot is feasible with the current inlet. A slot with twice the entrance area of the current slot was tested on this inlet and is reported in reference 5.

Large and small slots of similar size were also tested on another inlet and are reported in reference 2. This reference reports that doubling the slot size extended the bypass performance and increased the bypass mass-flow ratio from 0.09 to 0.18. The constant pressure stability index was increased from 14 to 20 percent. Reference 5 also reported gains in maximum bypass mass-flow ratio by doubling the slot size. Unfortunately, reference 5 also reports that the larger slot also suffered from a flow separation problem. Flow separated from the upstream slot surface near the slot leading edge. The problem is discussed at length in reference 5. Briefly, this separation existed for all minimum stable conditions and for supercritical conditions at the lower bypass airflows. The slot flow was not separated at the higher bypass flows at supercritical conditions. Thus, with the higher bypass exit areas, the separation would occur and grow in size as the inlet proceeded from supercritical to minimum stable. The separation changed the effective bypass exit area and controlled the slot airflow. Slot recovery and mass-flow ratio both decreased rather than increased as the inlet was operated from supercritical to minimum stable conditions. Because of the reversal in slot flow behavior the operation of a bypass exit control valve, such as the poppet valves of reference 4, might be unpredictable. Thus the usefulness of the higher mass-flow ratio region of the large slot bypass entrance which provides the high stability margin is in question.

A tendency of the slot flow to separate was also observed with the small slot. Figure 19 presents slot rake data and static-pressures distributions through the slot at the largest bypass exit area. These data indicate that the flow turned into the slot and remained well attached to the upstream slot wall only at supercritical inlet conditions.

Slot flow separation was also observed to occur in the good performing large slot of reference 2. In this case the size of the separation did not significantly change. It occurred at all inlet and slot flow conditions and no reversal of slot flow behavior was noted. Thus, schemes to reduce and/or stabilize the separated flow region in the slot bypass entrance of the current inlet might create a large slot configuration with stability performance as good as that of the porous configuration. Stabilization of the slot flow separation might be accomplished by bleeding flow from the slot upper surface just aft of the slot leading edge or by cutting back the slot leading edge to stabilize the separation at that location. This is worthwhile because of the construction advantages of a single slot over a porous surface composed of many holes.

Successful design of a large slot may also depend on factors other than slot flow separation. With small amounts of performance bleed as used herein for constant pressure stability index comparisons, the large slot bypass entrance of reference 5 degraded inlet performance. The rake data of reference 5 show that, without moderate amounts of bypass flow into the slot, the flow over the slot bypass entrance was seriously degraded and that a large low-energy boundary layer was formed. Such an occurrence did not happen with the large slot of reference 2. These contrasting results may be due to inlet design differences. With the inlet of this report and reference 5, the bypass

entrance was located in a region of varying Mach number, but with the inlet of refer-
ence 2 the Mach number over the slot region was almost constant.

An example of inlet internal static- and total-pressure distributions of the config-
urations reported herein is presented in figure 20 for minimum stable conditions. These
data were obtained with the distributed educated bypass entrance configuration and illus-
trate some typical results that appeared for all the bypass entrance types. The symbols,
incidently, are matched to those at minimum stable on the educated configuration per-
formance plots (fig. 14). Parts (a) and (b) of figure 20 show that the stability configura-
tions allowed the inlet terminal shock to travel well forward of the inlet throat at min-
imum stable conditions. Also, the centerbody pressure distributions at x/R_c of 2.9
to 3.3 inlet radii (fig. 20(b)) show a shock induced flow separation that was typical of
this inlet and first reported in reference 8. The separation was well forward of the inlet
throat and is also shown by the rake data of figure 20(c). The separated region was
rather small and the flow reattached before reaching the inlet throat (fig. 20(d)). Flow
was completely mixed by the time it reached the diffuser exit (fig. 20(f)).

The maximum angle of attack to which the inlet could be pitched and remain started
was determined for each stability bypass entrance configuration and is shown in part (b)
of figures 12 to 14. These data were obtained in a manner simulating normal inlet per-
formance bleed; that is, airflow was removed through the forward cowl and centerbody
bleed areas and no airflow was removed through the stability bypass. The point of inlet
operation before pitching the inlet to the unstart limit is indicated in each figure. Pres-
sure distributions on the leeward side of the inlet cowl and centerbody at the unstart
angle of attack are presented in figure 21 for supercritical inlet operation using the po-
rous stability bypass configuration. For reference, the pressure distributions at the 0
angle of attack initial inlet operating point are also shown. This figure, which is typical
of all configurations, shows that pitching the inlet to unstart angle of attack caused the
airflow forward of the inlet throat to be compressed to higher pressures. Specifically,
the cowl side pressures just aft of the forward cowl bleed indicate higher pressures than
sonic values. These data are in agreement with those of reference 13, which reports
that angle of attack unstarts for the same inlet were caused by local overcompression of
the flow to a subsonic condition forward of the throat on the leeward side of the inlet.

Because of the position of the stability bypass entrances aft of the overcompression
region it was thought unlikely that the presence of the bypass entrances could affect the
unstart angle. Indeed, the unstart angles of attack obtained herein of 3.3^o to 3.8^o are
in good agreement with the maximum unstart angles of about 3.6^o previously obtained for
this inlet in references 8 and 13. Thus the presence of the stability-bypass entrances
did not deteriorate the inlet angle of attack limits.

SUMMARY OF RESULTS

An experimental program was conducted in the Lewis 10- by 10-Foot Supersonic Wind Tunnel to evaluate the effectiveness of various types of stability bypass entrance configurations located in an inlet throat to provide an increased inlet stable airflow operating range. The inlet used in this investigation was an axisymmetric, mixed-compression type with 60 percent of the supersonic area contraction occurring internally at the design Mach number of 2.5. Three different stability-bypass entrance designs were tested: distributed porous, forward-slanted slot, and distributed educated slots. The following results were obtained:

1. A large stable airflow range can be provided for an inlet operating at a high performance condition by maintaining a constant pressure in the stability bypass plenum. From an initial inlet operating condition of 89 percent total-pressure recovery and a total cowl bleed mass-flow ratio of 0.02, each of the stability-bypass entrance types provided the inlet with a large stable airflow range (a constant pressure stability index greater than 15 percent). The largest stable airflow range (an index of 25.5 percent) was obtained using the distributed porous bypass entrance.

2. The cowl-side inlet-throat boundary layer was better controlled with the distributed porous bypass entrance. Other types of bypass entrances disturbed the throat flow and produced a thicker boundary layer.

3. Inlet unstart angle-of-attack tolerance was unaffected by the presence of the stability bypass entrances.

Lewis Research Center,
   National Aeronautics and Space Administration,
      Cleveland, Ohio, December 12, 1973,
         501-24.

APPENDIX - SYMBOLS

A   flow area, m^2

A_c cowl lip capture area, $0.1758 \ m^2$

AI   airflow index, $AI = 100 \left\{ 1 - \left[(W_{corr})_{min \ s} / (W_{corr})_{op} \right]_5 \right\}$, percent

D_5 steady state distortion, $\left[(P_{max} - P_{min}) / P_{av} \right]_5$

d   distance from local surface, cm

H   annulus or rake height, cm

L   axial distance from the upstream shoulder of the slot stability bypass, cm

M   Mach number

m/m_0 mass-flow ratio

P   total pressure, N/m^2

p   static pressure, N/m^2

R_c inlet cowl lip radius, 23.66 cm

r   radius, cm

SI_{cp} constant pressure stability index,
$$SI_{cp} = 100 \left\{ 1 - \left[(W_{corr})_{min \ s, cp} / (W_{corr})_{op} \right]_5 \right\}, \text{ percent}$$

W_{corr} corrected airflow, kg/sec

x   axial distance from cone tip, cm

α angle of attack, deg

θ_l cowl lip position parameter, $\tan^{-1} [1/(x/R_c)]$

φ circumferential position, deg

Subscripts:

av   average

bl   bleed

by   overboard bypass

cp   constant pressure

fc   forward cowl

l local

max   maximum

min   minimum

16

min s   minimum stable inlet operating point

op   inlet operating point

sb   stability bypass

un   unstart limit

x   value at distance x

0   free stream

5   diffuser exit station

REFERENCES

1. Sanders, Bobby W.; and Cubbison, Robert W.: Effect of Bleed-System Back Pressure and Porous Area on the Performance of an Axisymmetric Mixed-Compression Inlet at Mach 2.50. NASA TM X-1710, 1968.

2. Sanders, Bobby W.; and Mitchell, Glenn A.: Throat-Bypass Bleed Systems for Increasing the Stable Airflow Range of a Mach 2.50 Axisymmetric Inlet with 40-Percent Internal Contraction. NASA TM X-2779, 1973.

3. Sanders, Bobby W.; and Mitchell, Glenn A.: Increasing the Stable Operating Range of a Mach 2.5 Inlet. Paper 70-686, AIAA, June 1970.

4. Mitchell, Glenn A.; and Sanders, Bobby W.: Pressure-Activated Stability-Bypass-Control Valves to Increase the Stable Airflow Range of a Mach 2.5 Inlet with 40-Percent Internal Contraction. NASA TM X-2972, 1974.

5. Shaw, Robert J.; Mitchell, Glenn A.; and Sanders, Bobby W.: Distributed Porous Throat Stability Bypass to Increase the Stable Airflow Range of a Mach 2.5 Inlet with 60-Percent Internal Contraction. NASA TM X-2974, 1974.

6. Shaw, Robert J.; Mitchell, Glenn A.; and Sanders, Bobby W.: Distributed Educated Throat Stability Bypass to Increase the Stable Airflow Range of a Mach 2.5 Inlet with 60-Percent Internal Contraction. NASA TM X-2975, 1974.

7. Shaw, Robert J.; Mitchell, Glenn A.; and Sanders, Bobby W.: Forward-Slanted Slot Throat Stability Bypass to Increase the Stable Airflow Range of a Mach 2.5 Inlet with 60-Percent Internal Contraction. NASA TM X-2973, 1974.

8. Cubbison, Robert W.: Mealeason, Edward T.; and Johnson, David F.: Effect of Porous Bleed in a High Performance Axisymmetric, Mixed Compression Inlet at Mach 2.50. NASA TM X-1692, 1968.

9. Coltrin, Robert E.; and Calogeras, James E.: Supersonic Wind Tunnel Investigation of Inlet-Engine Compatibility. Paper 69-487, AIAA, June 1969.

10. McLafferty, George M.: A Stepwise Method for Designing Perforated Supersonic Diffusers. Rep. R-12133-5, United Aircraft Corp., Nov. 17, 1949.

11. McLafferty, George M.: A Study of Perforated Configurations for Supersonic Diffusers. Rep. R-53372-7, United Aircraft Corp., Dec. 1950.

12. McLafferty, George M.; and Ranard, E.: Pressure Losses and Flow Coefficients of Slanted Perforations Discharging from within a Simulated Supersonic Inlet. Rep. R-0920-1, United Aircraft Corp., 1958.

13. Choby, David A.: Tolerance of Mach 2.50 Axisymmetric Mixed-Compression Inlets to Upstream Flow Variations. NASA TM X-2433, 1972.

TABLE I. - INLET INTERNAL SURFACE COORDINATES

(a) Centerbody

Axial distance from cowl lip, x/R_c, inlet radii	Radial distance, r/R_c, inlet radii	Axial distance from cowl lip, x/R_c, inlet radii	Radial distance, r/R_c, inlet radii
0	0	4.402	0.609
(a)	(a)	4.563	.588
2.885	.640	4.724	.566
2.924	.649	5.161	.498
2.952	.655	5.261	.481
3.017	.667	5.361	.462
3.081	.678	5.461	.444
3.124	.684	5.561	.418
3.178	.691	5.661	.409
3.221	.696	5.761	.396
3.237	.700	5.861	.373
3.306	.703	5.961	.357
3.349	.705	6.061	.341
3.403	.707	6.161	.327
3.435	.708	6.261	.313
3.446		6.361	.299
3.457		6.461	.285
3.468		6.561	.272
3.478	.707	6.661	.260
3.489	.706	6.761	.250
3.543	.702	6.861	.243
3.596	.697	6.961	.240
3.650	.691	7.061	.239
3.865	.670	Cylinder	
3.972	.660		
4.079	.649	7.946	0.239
4.120	.644		
4.187	.636		
4.240	.635		
4.294	.623		

^{a}12.5^o Half angle conical section.

19

TABLE I. - Concluded. INLET INTERNAL SURFACE COORDINATES

(b) Cowl

Axial distance from cowl lip, x/R_c, inlet radii	Radial distance, r/R_c, inlet radii	Axial distance from cowl lip, x/R_c, inlet radii	Radial distance, r/R_c, inlet radii	Axial distance from cowl lip, x/R_c, inlet radii	Radial distance, r/R_c, inlet radii
2.009	1.000	3.446	0.952	5.461	0.913
2.156		3.457	.951	5.561	.916
2.297		3.468	.951	5.661	.917
2.383		3.478	.950	5.761	.918
2.469		3.489	.949	Cylinder	
2.491		3.543	.945		
2.512		3.596	.942	6.235	0.918
2.566	.999	3.650	.939	Bypass gap	
2.630	.997	3.756	.932		
2.695	.995	3.863	.925	6.845	0.887
2.738	.994	3.970	.919	6.861	.887
2.811	.992	4.088	.913	6.961	.885
2.860	.989	4.093	.913	7.061	.882
2.885	.988	4.189	.909	7.161	.879
2.924	.986	4.267	.906	7.261	.873
2.952	.985	4.277	.905	7.361	.868
3.017	.981	4.384	.903	7.461	.864
3.081	.979	4.545	.902	7.561	.863
3.124	.976	4.706	.902	7.661	.862
3.178	.972	4.868	.903	Cylinder	
3.221	.971	5.029	.904		
3.237	.966	5.093	.904	7.946	0.862
3.306	.963	5.161	.905		
3.350	.960	5.261	.907		
3.403	.955	5.361	.910		
3.435	.953				

TABLE II. - COWL-STATIC PRESSURE TAP
LOCATIONS ALONG TOP CENTERLINE

Axial distance from cowl lip, x/R_c, inlet radii		
Distributed porous configuration	Forward-slanted slot configuration	Educated configuration
2.983	2.983	2.983
3.090	3.090	3.090
3.160	3.160	3.194
3.195	3.195	3.203
3.230	3.230	3.257
3.264	3.265	3.310
3.300	3.298	3.364
3.335	3.343	3.418
3.369	3.389	3.471
3.404	3.566	3.525
3.439	3.589	3.579
3.474	3.621	3.620
3.509	3.662	3.662
3.544	3.739	3.739
3.579	3.818	3.818
3.620	3.961	3.961
3.662	4.254	4.254
3.739		
3.818		
3.961		
4.254		

TABLE III. - CENTERBODY STATIC
PRESSURE TAP LOCATIONS ALONG
TOP CENTERLINE

Axial distance from cowl lip, x/R_c, inlet radii		
2.806	3.367	3.854
2.920	3.402	3.906
3.022	3.440	3.961
3.135	3.470	4.067
3.173	3.516	4.174
3.206	3.573	4.331
3.242	3.635	
3.272	3.691	
3.315	3.741	
3.332	3.798	

(a) Front view.

Choked plug assemblies for centerbody bleed flow

Centerbody bleed pipe (1 of 2)

Choked plug assembly for diffuser-exit flow

Stability-bypass pipe (1 of 2)
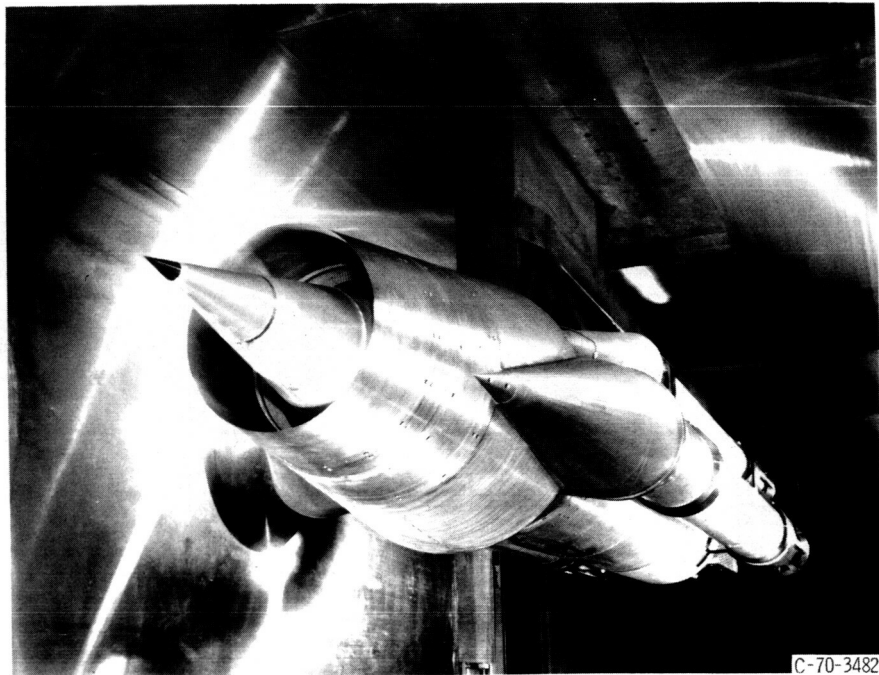
Choked plug assemblies for stability-bypass flow
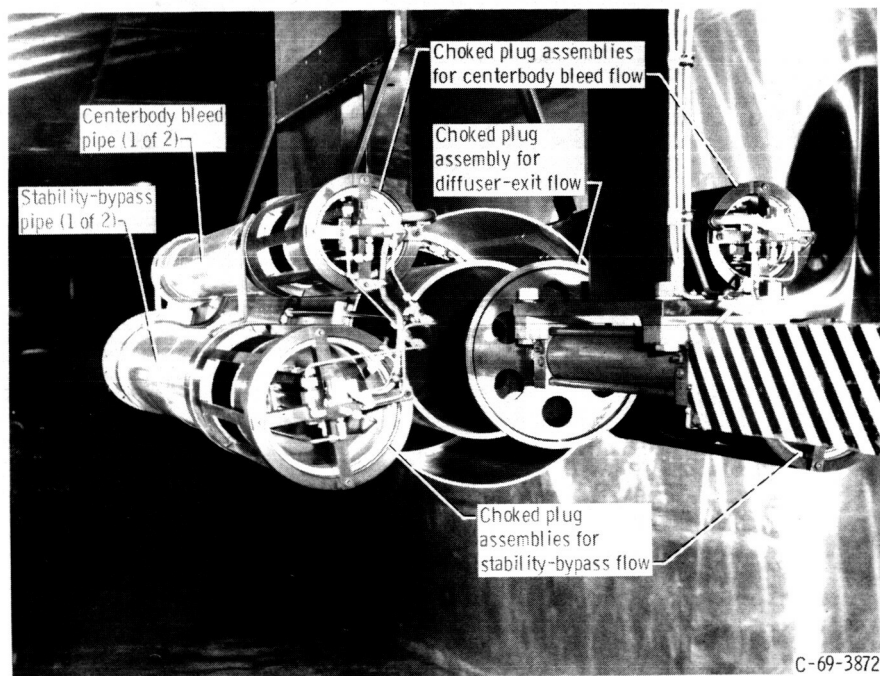
(b) Rear view.

Figure 1. - Model installed in wind tunnel.

22

Static-pressure ratio, p_x/p_0

Mach number, M_x

M_x

p_x/p_0

Compensation for boundary-layer bleed

p_x/p_0

M_x

Cowl surface conditions

Radial distance, x/R_c, inlet radii

$M_0 = 2.50$

$M_{av} = 0.8125$, $(P/P_0)_{av} = 0.975$

$M_{av} = 1.239$, $(P/P_0)_{av} = 0.988$

Inlet contour

Static-pressure ratio, p_x/p_0

Mach number, M

M_x

p_x/p_0

p_x/p_0

M_x

Axial distance from cone tip, x/R_c, inlet radii

Centerbody surface conditions
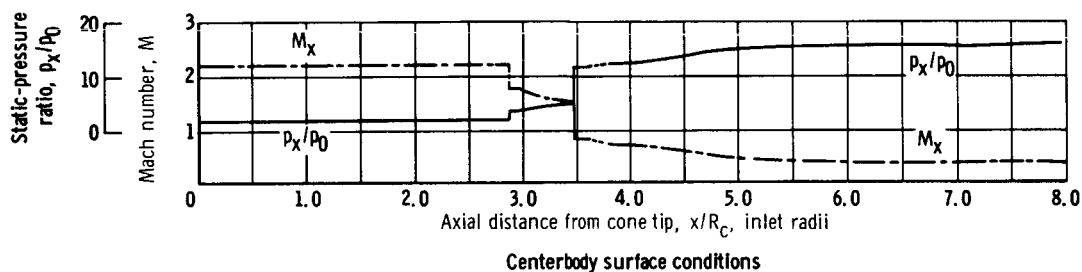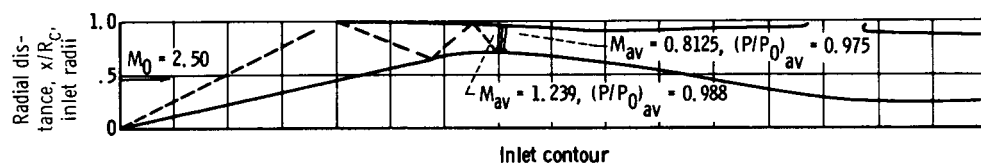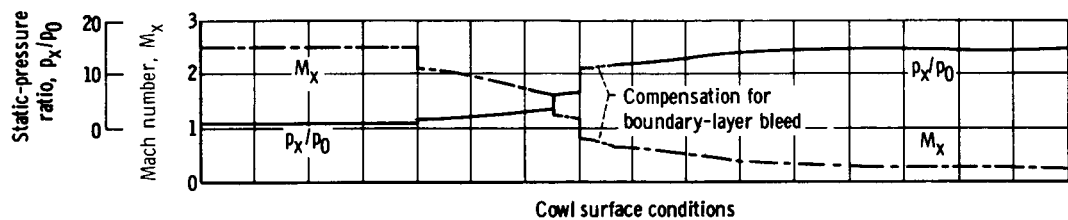
(a) Inlet dimensions and theoretical flow conditions.

Flow area ratio, A_x/A_c

Cowl lip

Overboard by-pass opening

Compressor face

Fixed region

Translating region

Throat region

Centerbody support struts

Axial distance from cone tip, x/R_c, inlet radii
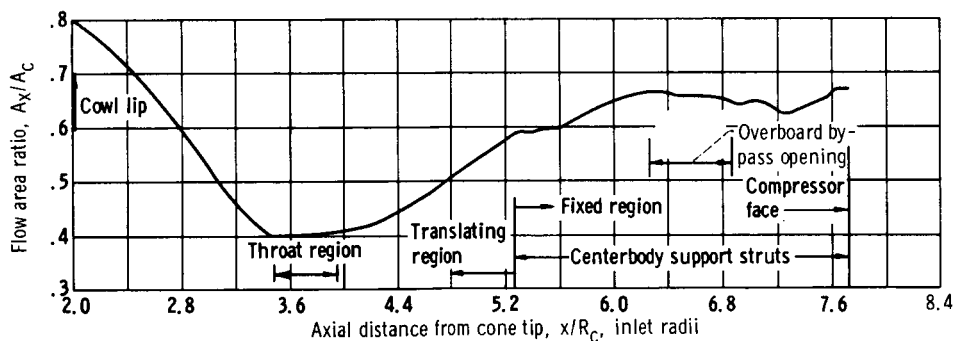
(b) Diffuser area variation for θ_l, 26.72^0.

Figure 2. – Aerodynamic details.

| Station | 0 | | 47.52 | 78.43 | 93.70
3.960 | 98.07 | 124.54 | | 174.98 | 182.55
7.716 |
| Axial distance, x/R_c | | | 2.009 | 3.315 | | 4.145 | 5.264 | | 7.396 | |
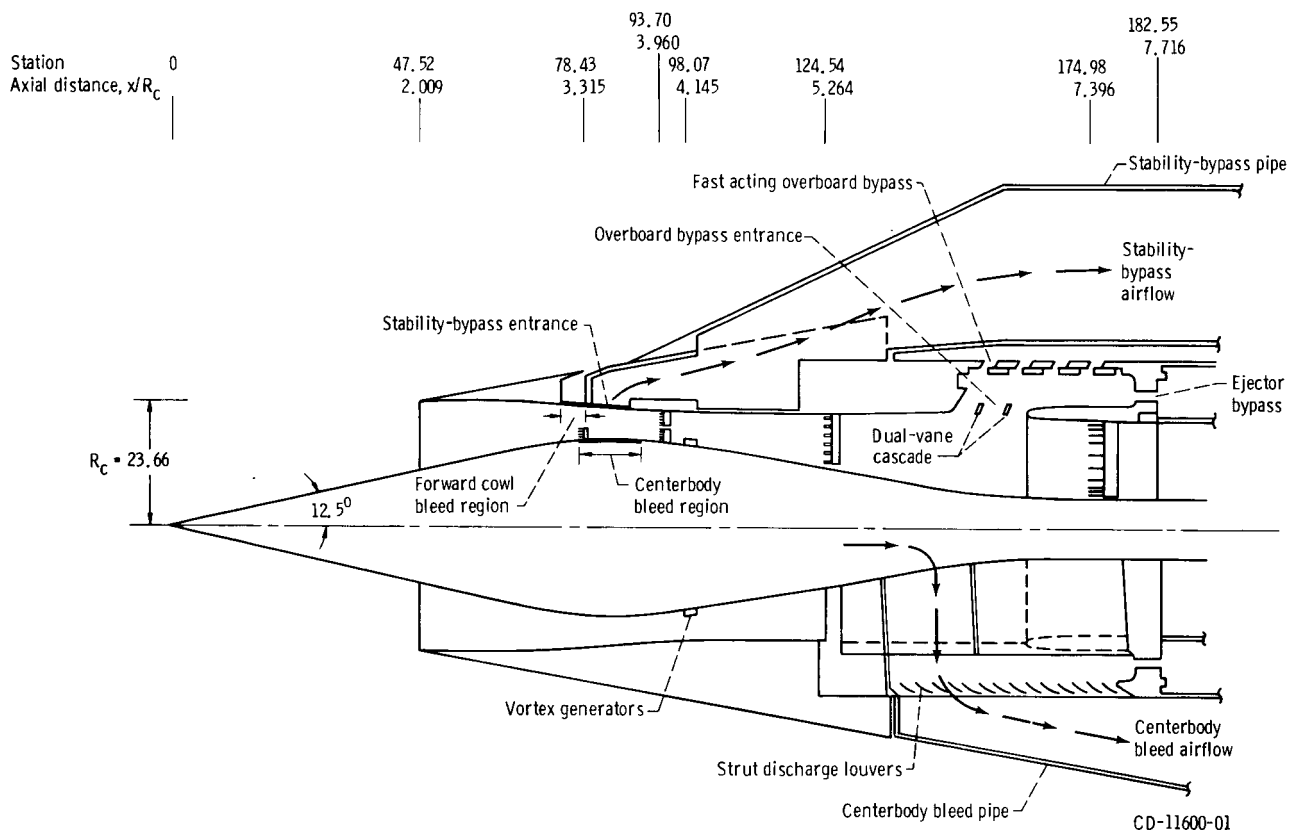
Figure 3. – Inlet details. (All linear dimensions are in cm.)

CD-11600-01

$R_c = 23.66$

12.5^0

Fast acting overboard bypass

Overboard bypass entrance

Stability-bypass pipe

Stability-bypass airflow

Stability-bypass entrance

Ejector bypass

Forward cowl bleed region

Centerbody bleed region

Dual-vane cascade

Vortex generators

Strut discharge louvers

Centerbody bleed pipe

Centerbody bleed airflow

24

Leading edge,
0.0254 rad

Upper surface coordinates
from NACA 0012 airfoil
(lower surface is flat)

0.1524

2.54

1.27

Generator detail

Cowl

Diffuser-exit total-
pressure rakes

C D C D C D C

D D

Converging
pair (C)

Diverging
pair (D)

Centerline of
centerbody
support struts

Looking downstream

Flow

16°

3.95   3.95

Generator detail

Figure 4. - Vortex generator design. (All linear dimensions are in cm.)

Overboard
bypass flow

Forward cowl
bleed flow

Forward cowl
bleed region

Stability-bypass
entrance

Stability-bypass flow

Stability-
bypass pipe
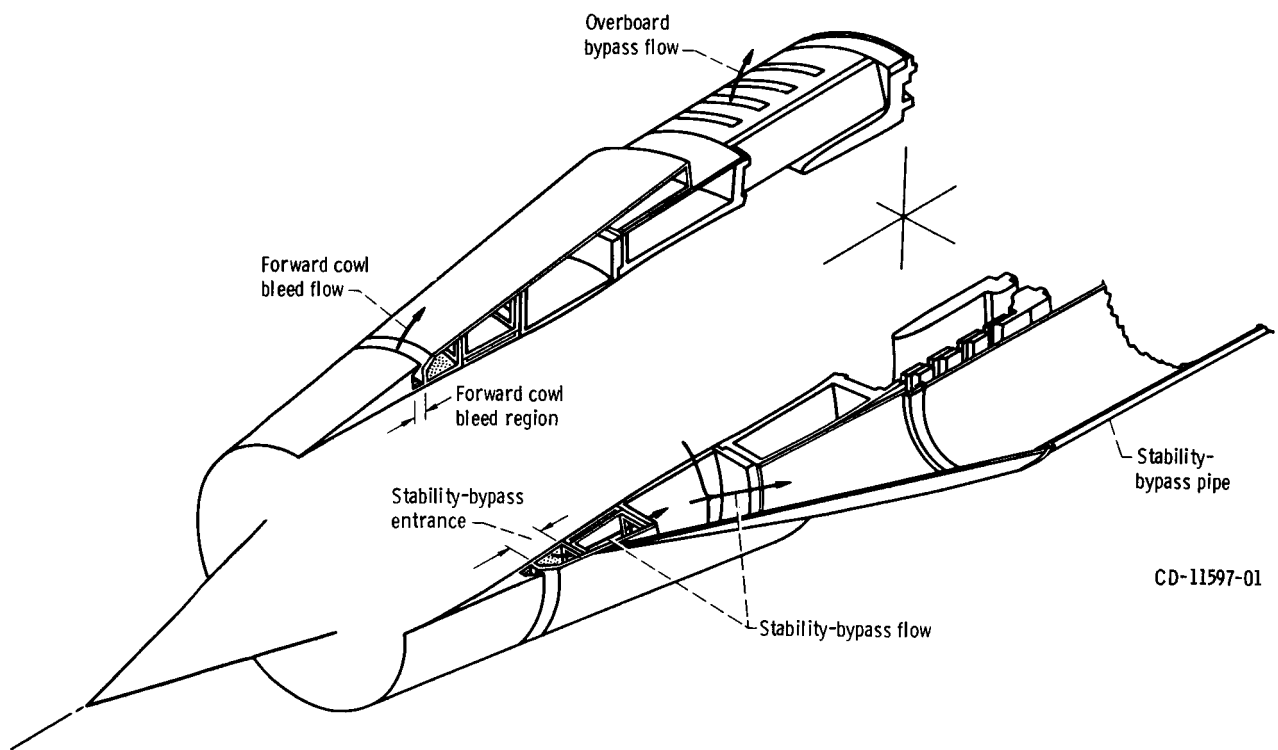
CD-11597-01

Figure 5. - Sketch of inlet cowl showing cowl bleed and bypass ducting.

(a) Distributed porous stability-bypass entrance. Hole diameter, 0.3175 centimeter.

(b) Forward-slanted slot stability-bypass entrance.

(c) Distributed educated stability-bypass entrance.
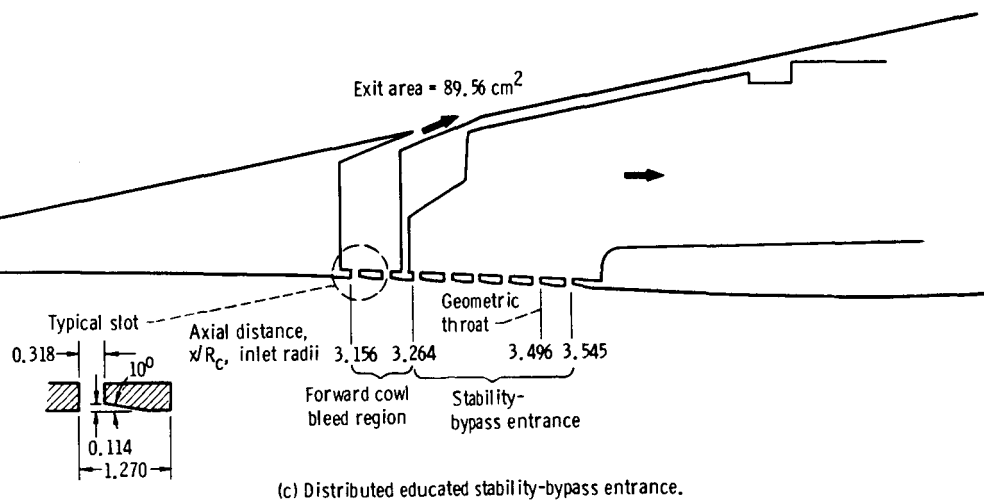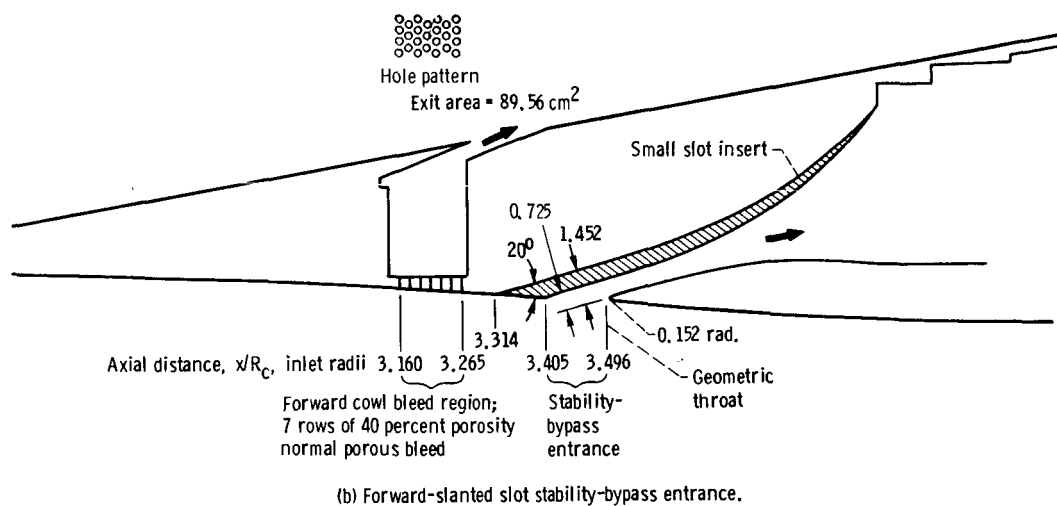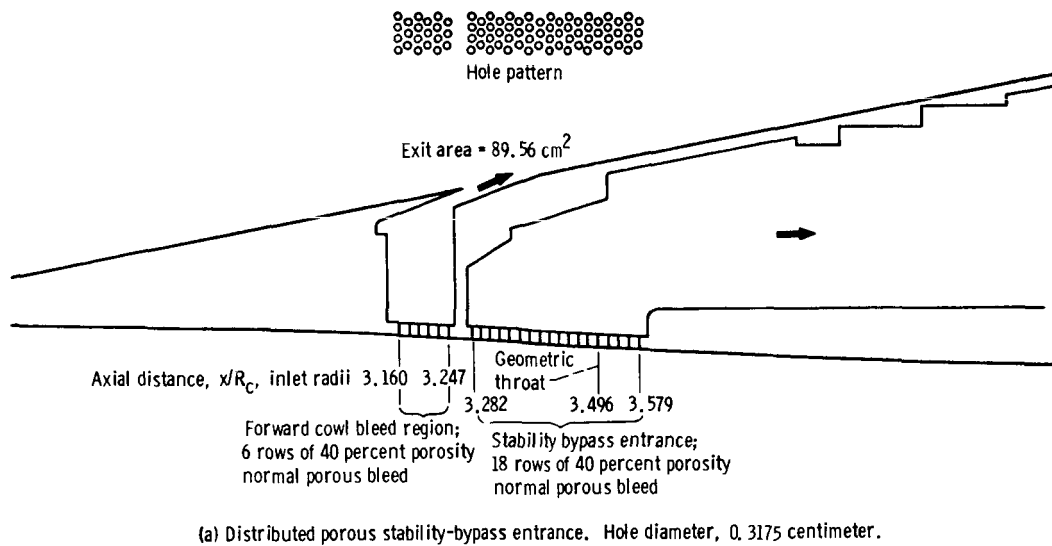
Figure 6. - Forward cowl bleed and stability-bypass entrance arrangements. (Dimensions are in cm unless otherwise noted.)

Geometric throat

Theoretical shock pattern

Air flow

Experimental shock pattern

Distributed porous

Forward slanted slot

Distributed educated

Bypass entrance type	Forward cowl bleed region	Stability-bypass entrance	Centerbody bleed region
Distributed porous	■ ■ ■ □ □ □	● ● ● ● ● ● □ □ □ □ □ □ □ □ □ □ □ □ □ □	□ □ □ □ □ □ ■ ■ ■ ■
Forward-slanted slot	● ● ● □ □ □		● ● ● □ □ □ ■ ■ ■ ■
Distributed educated	▽	▽ ▽ ▽ ▽ ▽	□ □ □ □ □ □ ■ ■ ■ ■

□ Hole row open   ▽ Educated slot open
■ Hole row closed   ▼ Educated slot closed

Figure 8. - Inlet stability-bypass entrance and bleed region configurations.

Airflow

Geometric throat
3.475

Axial distance, x/R$_c$, inlet radii   3.315   3.349   3.385   3.367   3.402   3.419   3.438   3.504   3.553   3.602   3.702   3.800

Figure 7. - Centerbody bleed arrangement. Hole diameter, 0.3175 centimeter.

○ Total-pressure probe
● Static-pressure tap

Boundary-layer rake; $\varphi = -10°$; $x/R_c = 3.315$

H = 6.112 cm

d/H
—0.187
— .125
— .083
— .024
— .017

Centerbody

Throat exit rake; $\varphi = 10°$; $x/R_c = 3.960$

Cowl

H = 6.112 cm

d/H
—0.975 .926
— .860
— .784
— .709
— .635
— .433
— .349
— .266
— .179 .092
— .029

Centerbody

Mid-diffuser rake; $\varphi = 10°$; $x/R_c = 5.264$

Cowl

H = 10.239 cm

d/H
—0.940
— .815
— .650
— .490
— .320
— .110

Centerbody

Typical diffuser exit rake; $x/R_c = 7.396$

Cowl

H = 14.905 cm

d/H
—0.982 .945
— .907
— .829
— .699
— .552
— .378
— .236
— .151
— .047

Centerbody
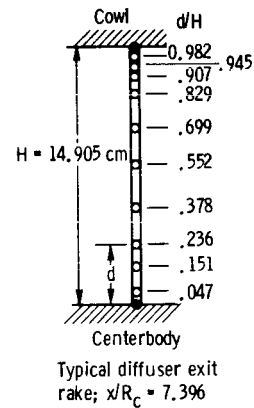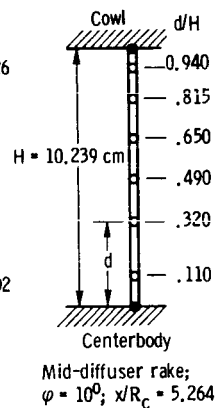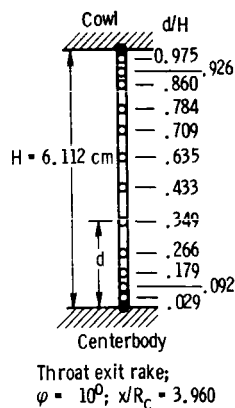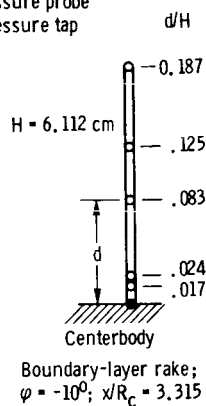
(a) Inlet-total-pressure rake dimensions.

Downstream view

$0°$

Rake 5, 332.5°

Rake 6, 27.5°

Strut centerline

Rake 4, 267.5°

Rake 1, 92.5°

Rake 3, 212.5°

Rake 2, 147.5°

Hollow centerbody support struts
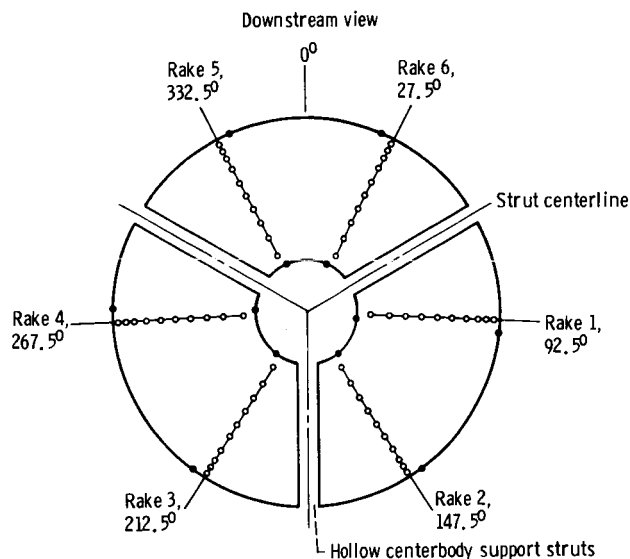
(b) Total- and static-pressure instrumentation at diffuser-exit station, $x/R_c = 7.396$.

Total

Static

Forward cowl pressure probes

Stability-bypass total-pressure rakes $\varphi = 90°$, $270°$

Axial distance, x/R_c, 4.086

Overboard bypass plenum total-pressure probe

Centerbody base total-pressure probe

CD-11611-01
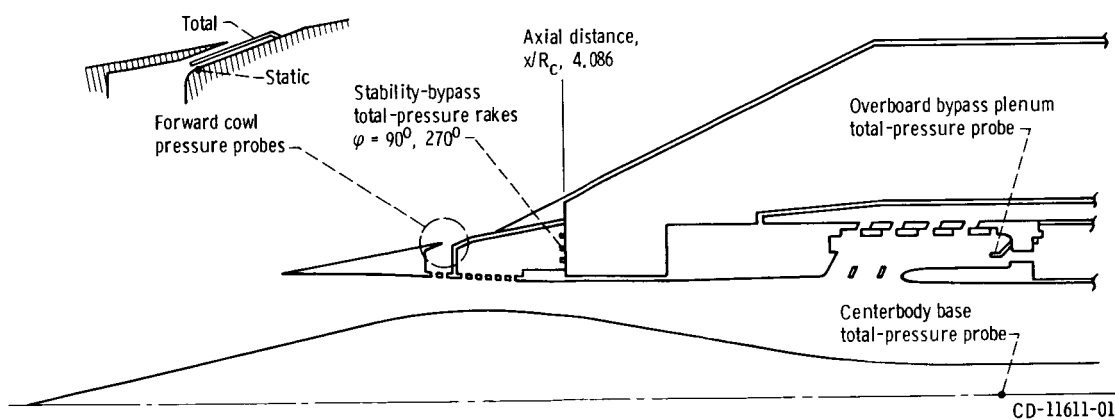
(c) Bleed and bypass pressure instrumentation.

Figure 9. – Inlet-pressure instrumentation (x/R_c is the axial distance from cone tip, φ is the circumferential position, and d/H is the ratio of distance from surface to annulus height).

Slot static-pressure tap
locations along top centerline

Tap	L/R_c	Tap	L/R_c
1	-0.106	8	0.168
2	-.062	9	.228
3	-.016	10	.308
4	.016	11	.390
5	.061	12	.478
6	.087	13	.173
7	.127		
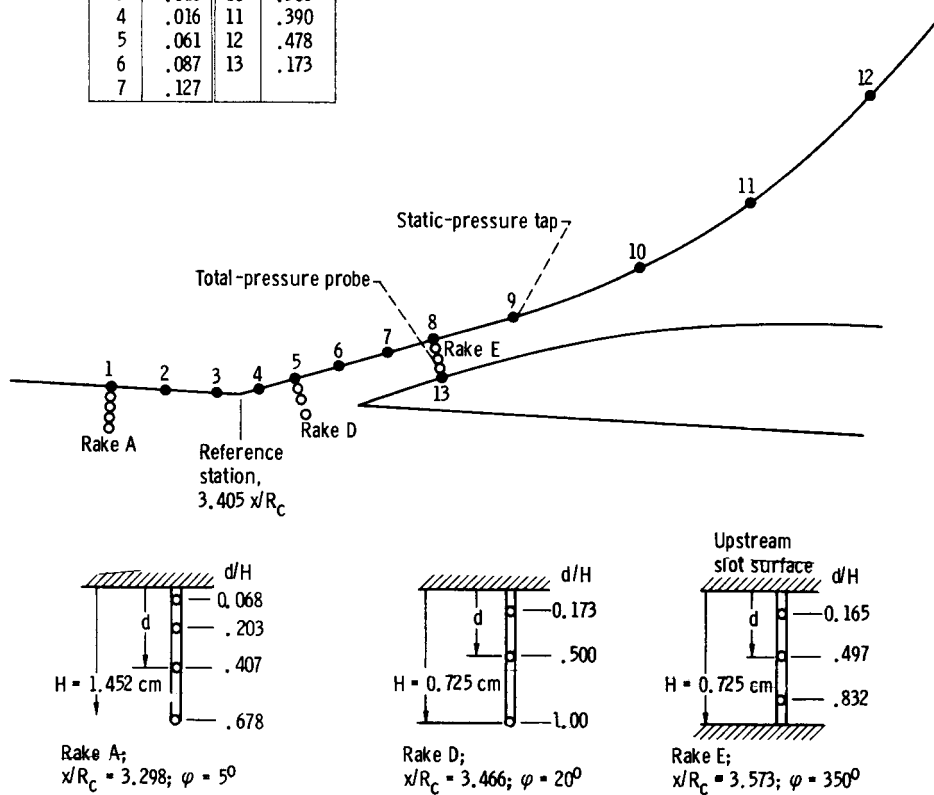
Figure 10. – Forward-slanted-slot pressure instrumentation.

(a) Stability bypass performance.

(b) Inlet performance.

(c) Airflow index.
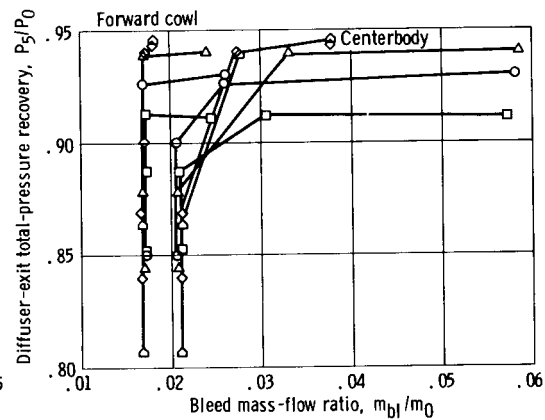
(d) Stability index for constant stability-bypass recovery.

(e) Variation of constant-pressure stability index with diffuser-exit total-pressure recovery.

(f) Constant-pressure stability index for chosen inlet-total-pressure recovery.

(g) Inlet performance for point J as match condition and with constant-pressure bypass-exit control on stability-bypass airflow.

Figure 11. - Inlet stability data.

(a) Stability-bypass performance.

(b) Inlet performance.

(c) Airflow index.

(d) Stability index for constant stability-bypass recovery.
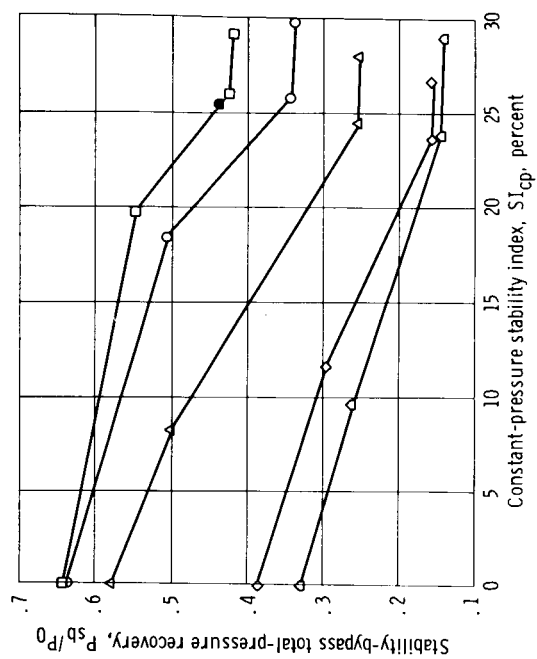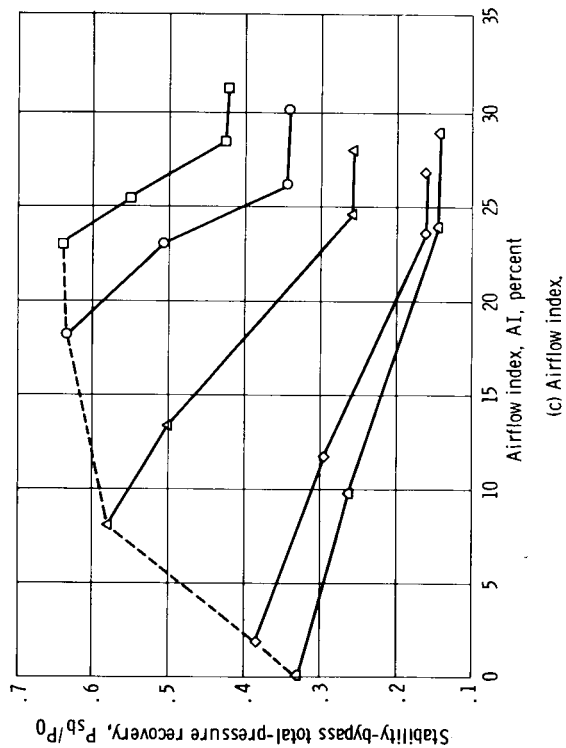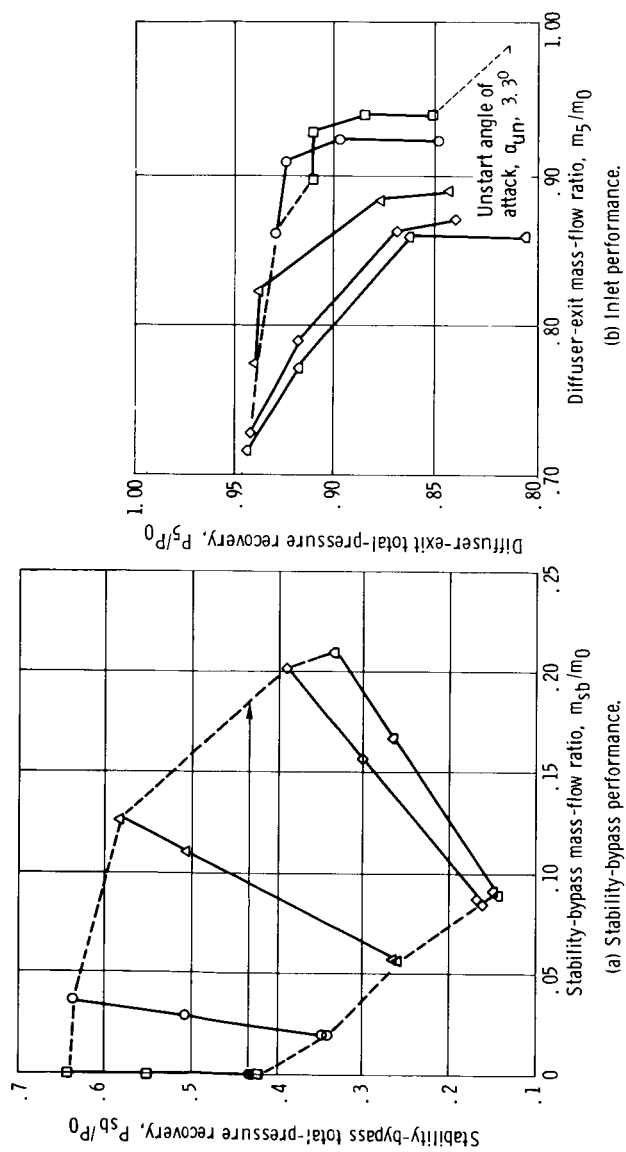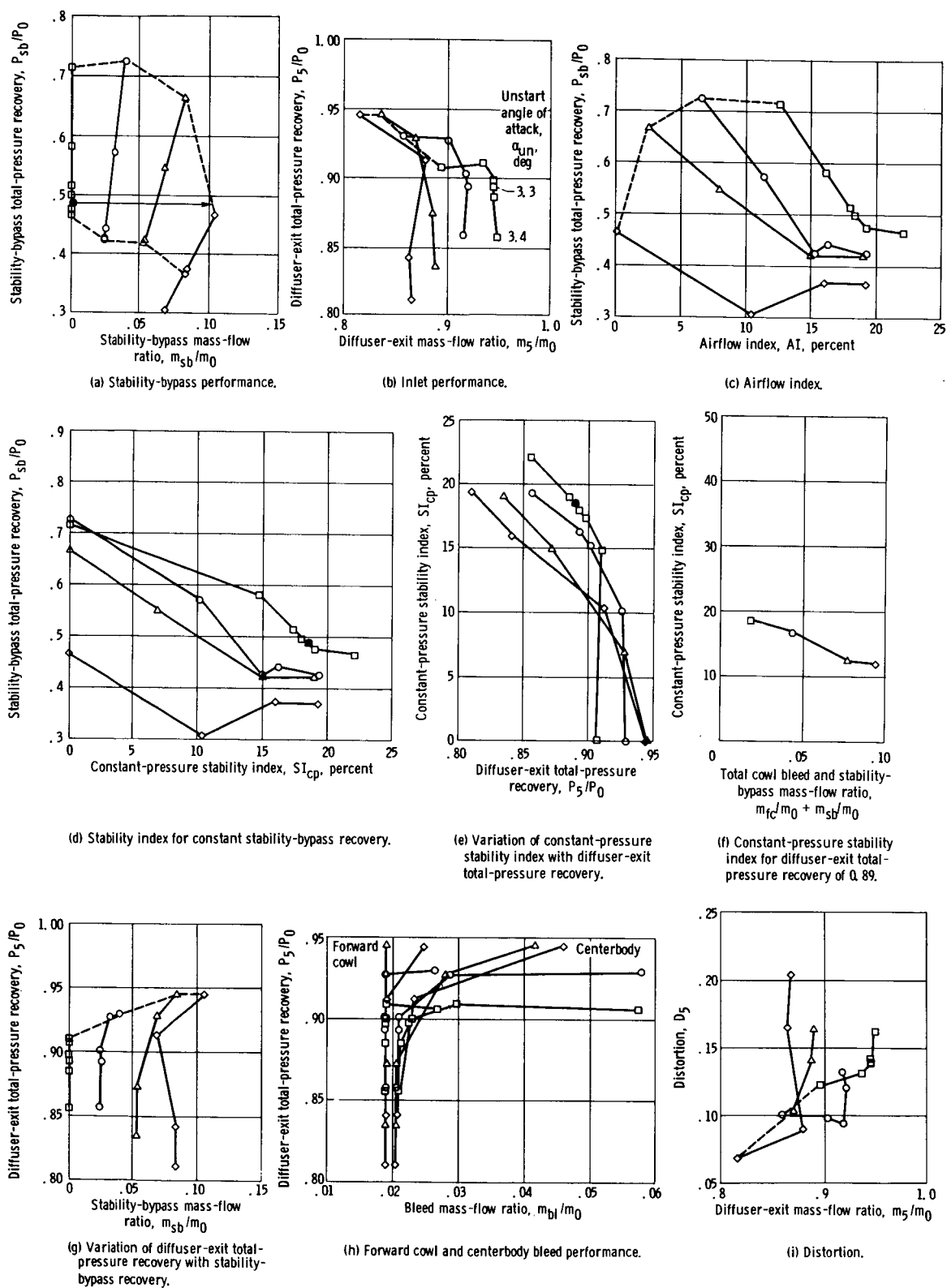
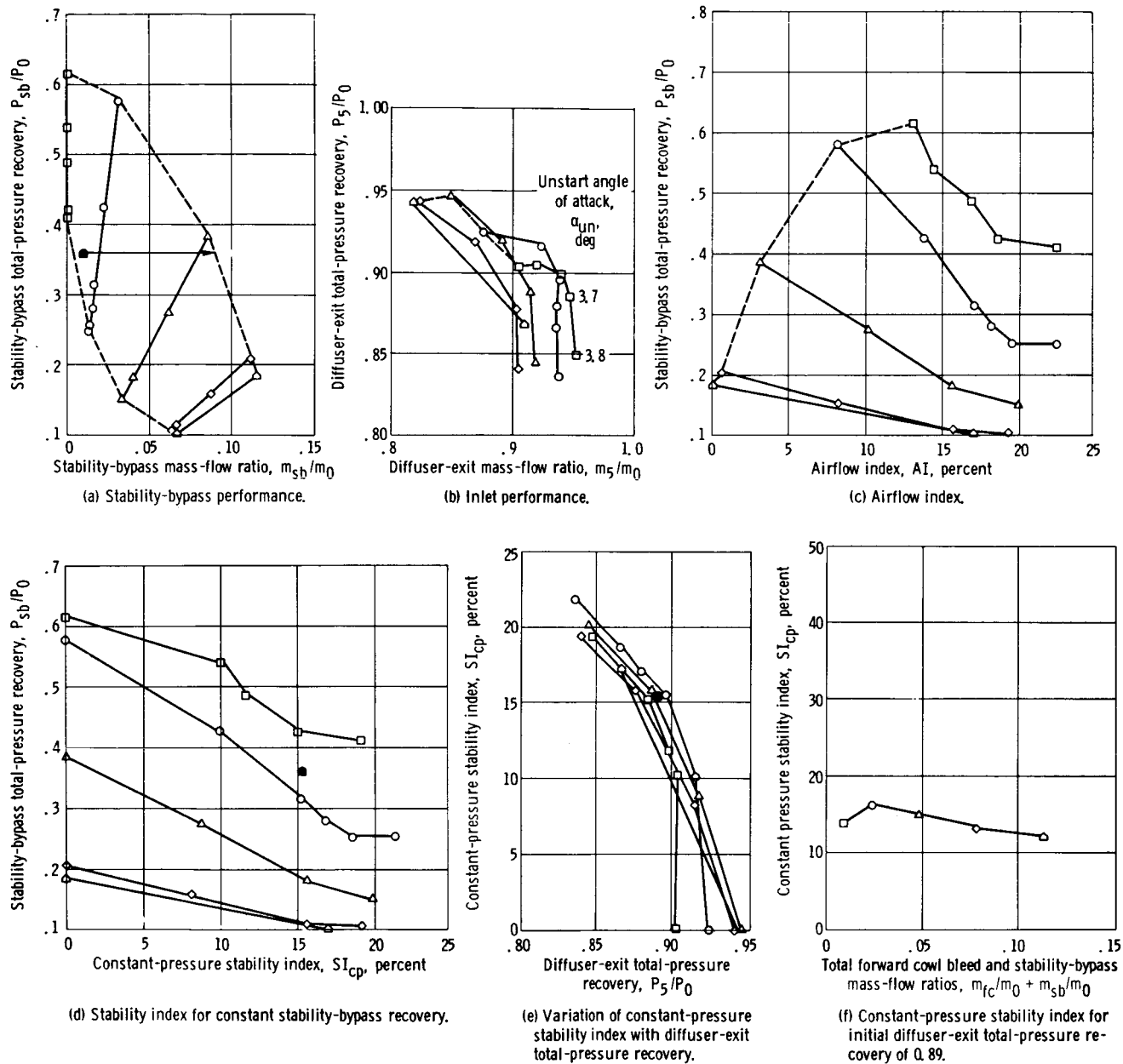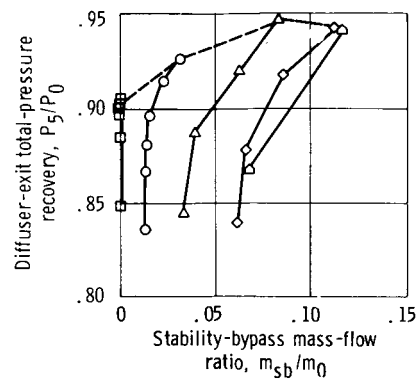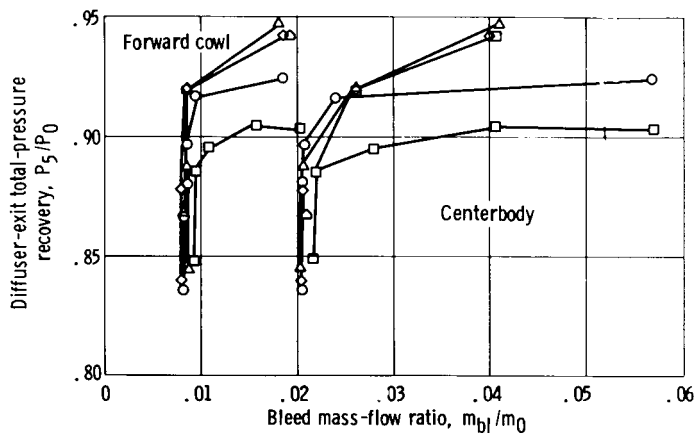Figure 12. - Performance of distributed porous configuration. Free-stream Mach number, 2.5; angle of attack, 0°; overboard-bypass mass-flow ratio, 0.01.
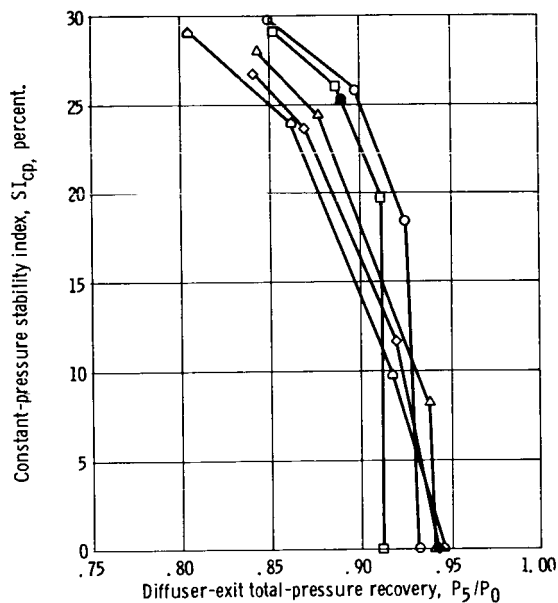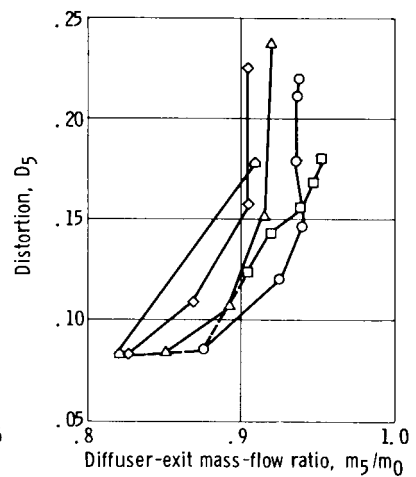
(e) Variation of constant-pressure stability index with diffuser-exit total-pressure recovery.
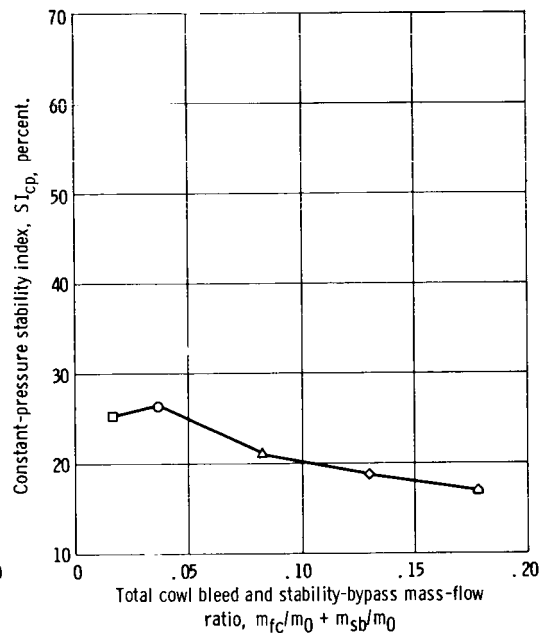
(f) Constant-pressure stability index for initial diffuser-exit total-pressure recovery of 0.89.
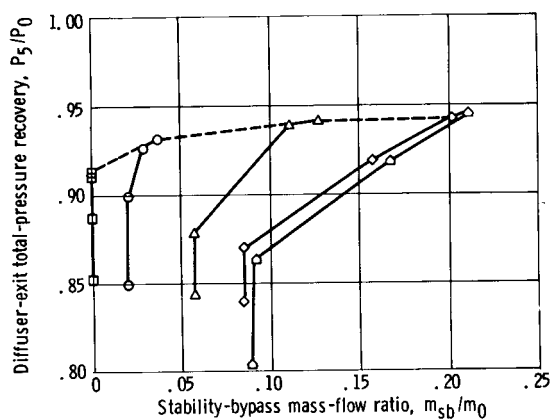
(g) Variation of diffuser-exit total-pressure recovery with stability-bypass mass flow.

(h) Forward cowl and centerbody bleed performance.
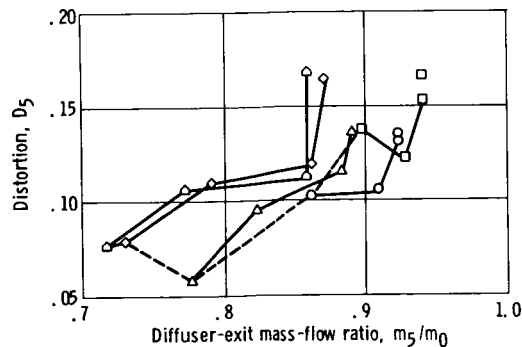
(i) Steady-state distortion.

Figure 12. - Concluded.

(a) Stability-bypass performance.

(b) Inlet performance.

(c) Airflow index.

(d) Stability index for constant stability-bypass recovery.

(e) Variation of constant-pressure stability index with diffuser-exit total-pressure recovery.

(f) Constant-pressure stability index for diffuser-exit total-pressure recovery of 0.89.

(g) Variation of diffuser-exit total-pressure recovery with stability-bypass recovery.

(h) Forward cowl and centerbody bleed performance.

(i) Distortion.

Figure 13. - Performance of small forward-slanted slot configuration. Free-stream Mach number, 2.5; angle of attack, 0^0; overboard-bypass mass-flow ratio, 0.01.

34

(a) Stability-bypass performance.

(b) Inlet performance.

(c) Airflow index.

(d) Stability index for constant stability-bypass recovery.

(e) Variation of constant-pressure stability index with diffuser-exit total-pressure recovery.

(f) Constant-pressure stability index for initial diffuser-exit total-pressure recovery of 0.89.

Figure 14. - Performance of distributed educated configuration. Free-stream Mach number, 2.5; angle of attack, 0^0; overboard-bypass mass-flow ratio, 0.01.

(g) Variation of diffuser-exit total-pressure recovery with stability-bypass mass flow.

(h) Forward cowl and centerbody bleed performance.

(i) Distortion.

Figure 14. - Concluded.
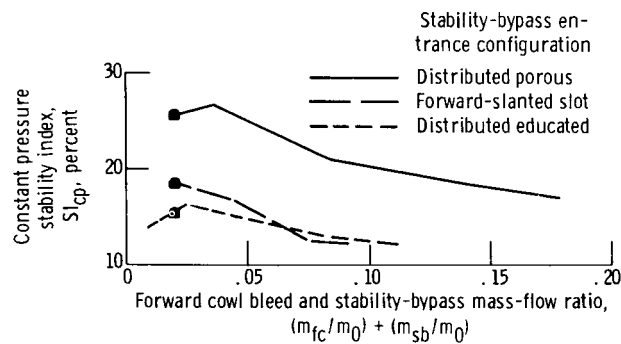
Figure 15. - Constant-pressure stability index for an inlet diffuser-exit total-pressure recovery of 0.89.
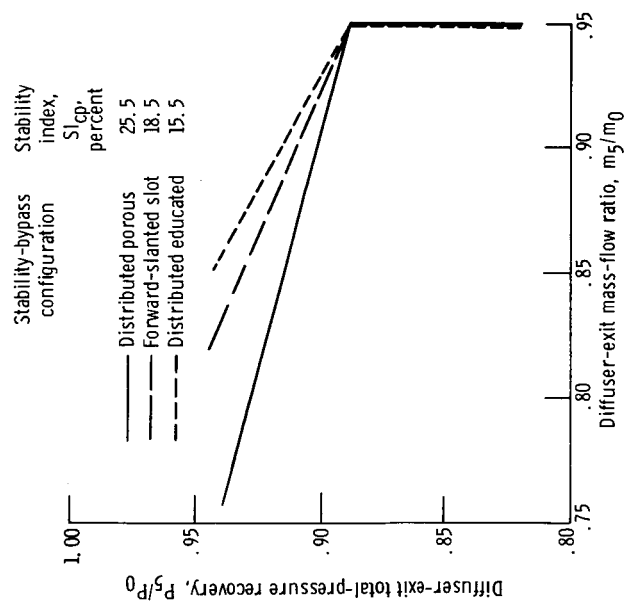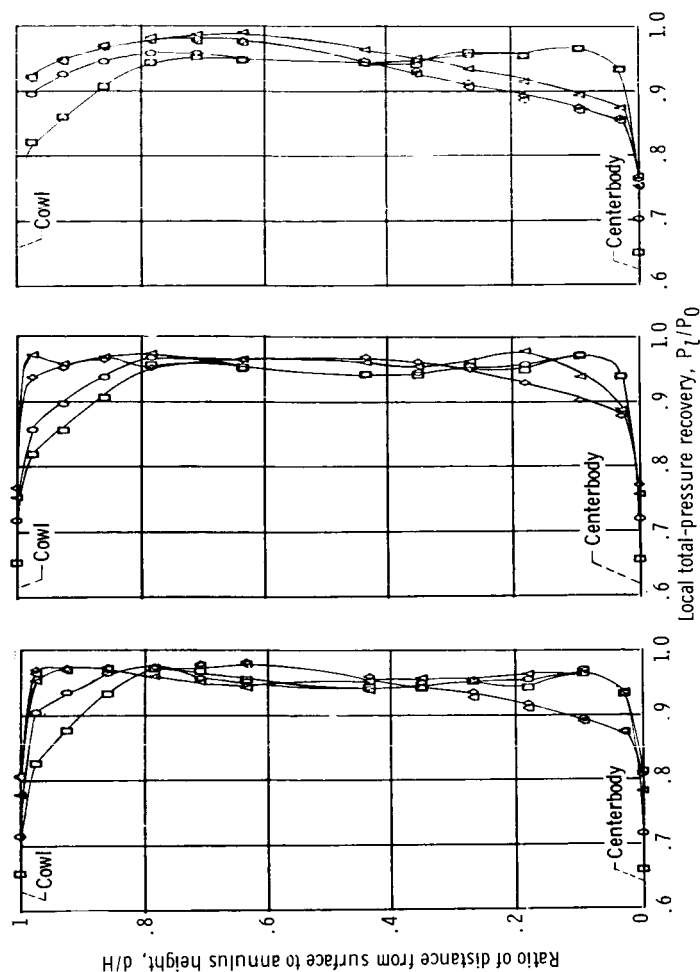
36

Figure 17 (Throat exit rake profiles)

Ratio of distance from surface to annulus height, d/H

(a) Distributed porous configuration.

Mass-flow ratio, m_5/m_0	Total-pressure recovery, P_5/P_0	P_{sb}/P_0
0.898	0.912	0.641
.862	.931	.635
.776	.941	.581
.729	.943	.387
.717	.945	.331

Symbols at 0 and 1.0 d/H indicate static pressures.

(b) Forward-slanted slot configuration.

Mass-flow ratio, m_5/m_0	Total-pressure recovery, P_5/P_0	P_{sb}/P_0
0.896	0.907	0.715
.859	.929	.726
.836	.945	.665
.816	.944	.464

Symbols at 0 and 1.0 d/H indicate static pressures.

(c) Distributed educated configuration.

Mass-flow ratio, m_5/m_0	Total-pressure recovery, P_5/P_0	P_{sb}/P_0
0.905	0.903	0.615
.876	.924	.580
.850	.946	.385
.824	.942	.209
.819	.942	.185

Symbols at 0 and 1.0 d/H indicate static pressures.

Local total-pressure recovery, P_l/P_0

Figure 17. – Throat exit rake profiles at minimum stable conditions.

Figure 16

Diffuser-exit total-pressure recovery, P_5/P_0

Diffuser-exit mass-flow ratio, m_5/m_0

Stability-bypass configuration	Stability index, SI_{cp}, percent
Distributed porous	25.5
Forward-slanted slot	18.5
Distributed educated	15.5

Figure 16. - Inlet performance based on constant stability-bypass recovery to unstart limit from initial inlet conditions of 89 percent total-pressure recovery and forward cowl bleed and stability mass-flow ratio of 0.02. Free-stream Mach number, 2.5; angle of attack, 0^0; overboard-bypass mass-flow ratio, 0.01.

Figure 18. – Throat exit rake profiles at supercritical conditions.

Figure 19. – Forward-slanted slot static- and total-pressure distributions at the largest stability bypass exit area.
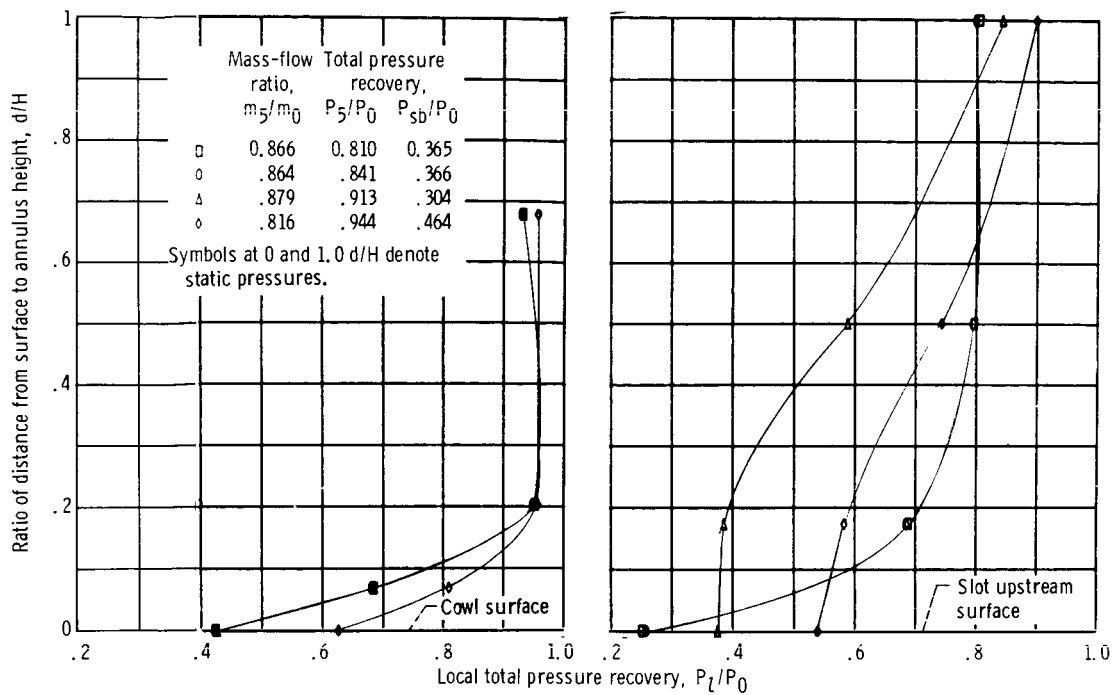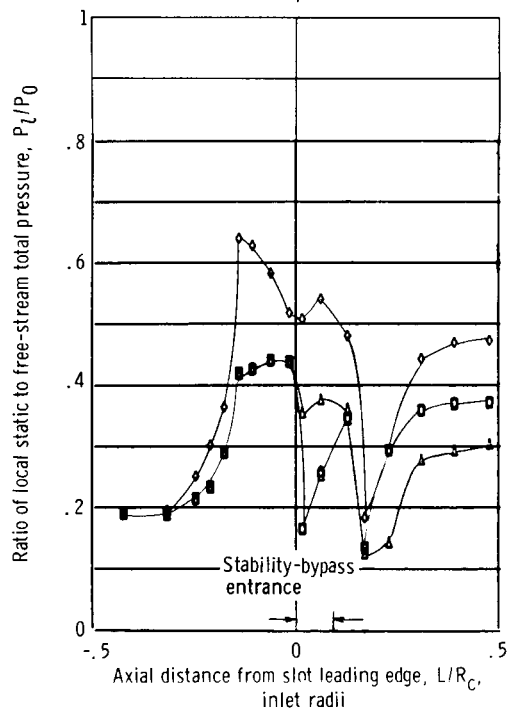
(a) Slot rake A profiles.

(b) Slot rake D profiles.
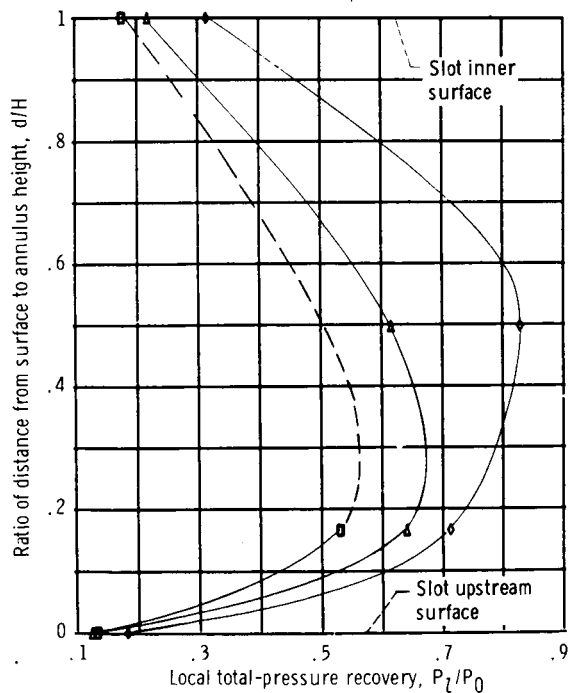
(c) Slot rake E profiles.

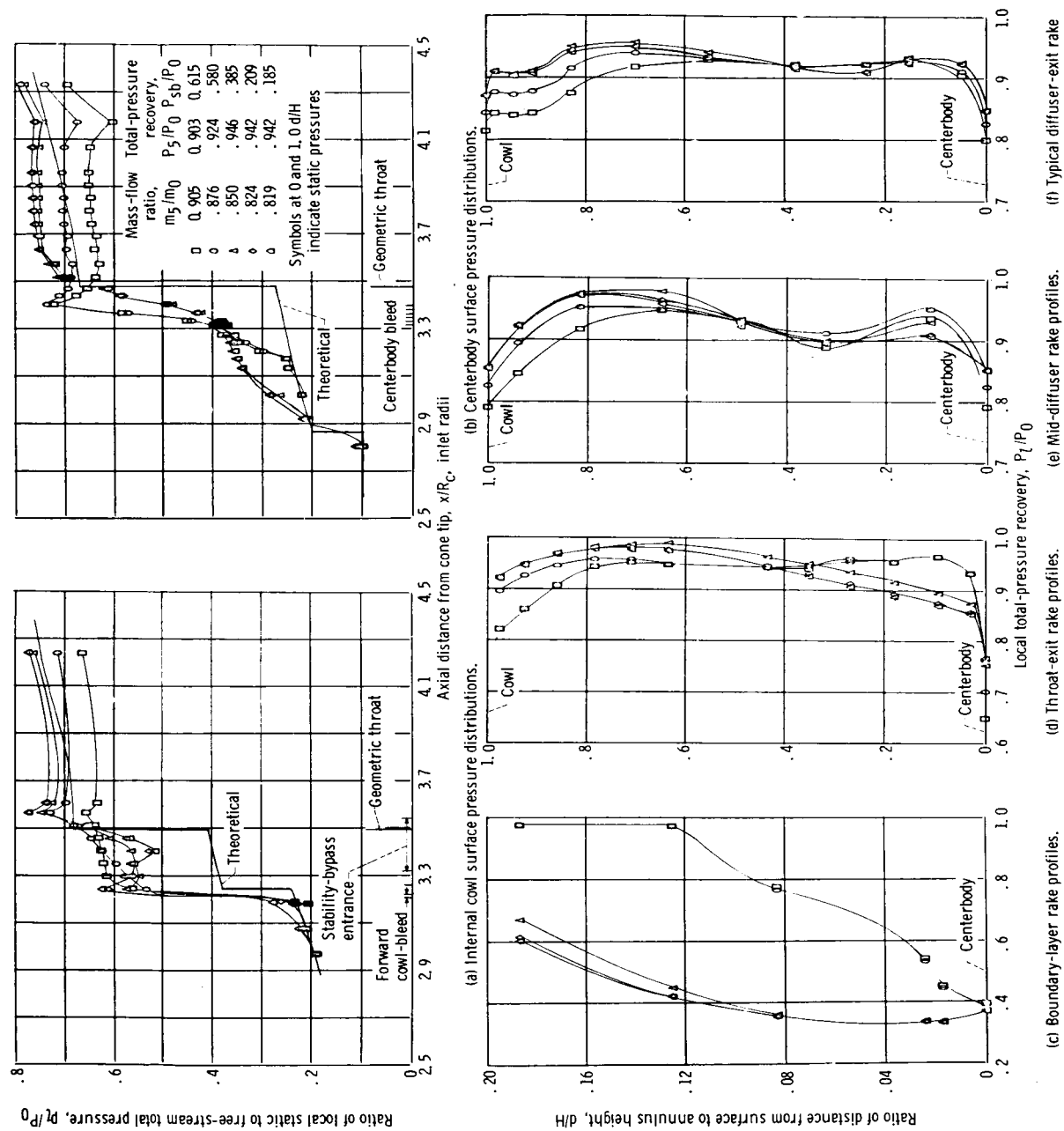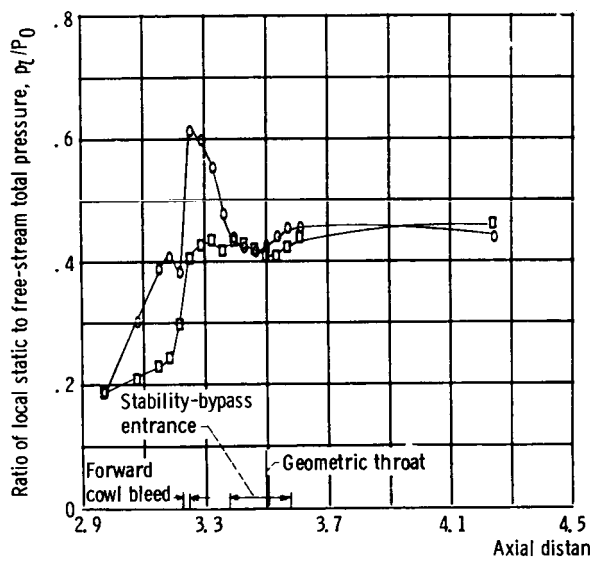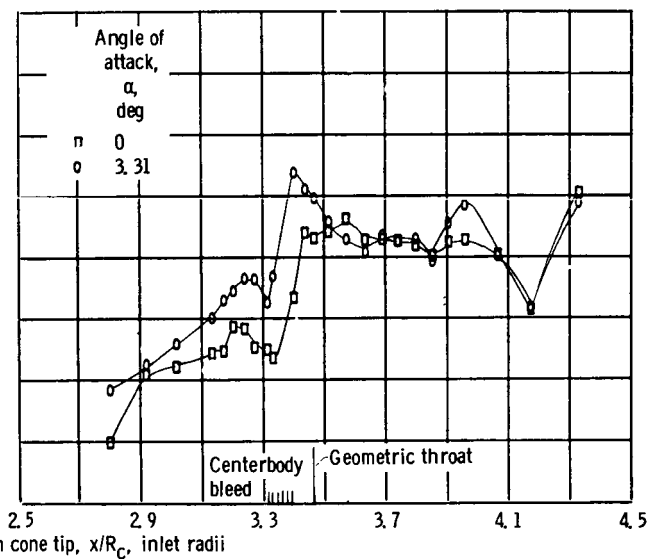(d) Surface pressure distributions on upstream surface of forward-slanted slot.

Figure 20. – Diffuser static- and total-pressure distributions for distributed educated configuration at minimum stable operation.

40

(a) Internal cowl surface pressure distributions.

(b) Centerbody surface pressure distributions.

Figure 21. – Static pressure distributions at 0° angle of attack and maximum angle of attack prior to unstart. Distributed porous configuration.